



This is a repository copy of *Stability analysis of DC micro-grids with CPLs under novel decentralized primary and distributed secondary control*.

White Rose Research Online URL for this paper:

<https://eprints.whiterose.ac.uk/181684/>

Version: Accepted Version

Article:

Braitor, A.-C. orcid.org/0000-0002-7666-0457, Konstantopoulos, G. and Kadiramanathan, V. (2022) Stability analysis of DC micro-grids with CPLs under novel decentralized primary and distributed secondary control. *Automatica*, 139. 110187. ISSN 0005-1098

<https://doi.org/10.1016/j.automatica.2022.110187>

Article available under the terms of the CC-BY-NC-ND licence
(<https://creativecommons.org/licenses/by-nc-nd/4.0/>).

Reuse

This article is distributed under the terms of the Creative Commons Attribution-NonCommercial-NoDerivs (CC BY-NC-ND) licence. This licence only allows you to download this work and share it with others as long as you credit the authors, but you can't change the article in any way or use it commercially. More information and the full terms of the licence here: <https://creativecommons.org/licenses/>

Takedown

If you consider content in White Rose Research Online to be in breach of UK law, please notify us by emailing eprints@whiterose.ac.uk including the URL of the record and the reason for the withdrawal request.



eprints@whiterose.ac.uk
<https://eprints.whiterose.ac.uk/>

Stability analysis of DC micro-grids with CPLs under novel decentralised primary and distributed secondary control [★]

A.-C. Braitor ^a, G.C. Konstantopoulos ^{a,b}, V. Kadiramanathan ^a

^a*Department of Automatic Control and Systems Engineering, University of Sheffield, Sheffield S1 3JD, United Kingdom*

^b*Department of Electrical and Computer Engineering, University of Patras, Rion 26504, Greece*

Abstract

This paper investigates the stability of meshed DC micro-grids with constant power loads (CPLs), under decentralised primary and distributed secondary control scheme to achieve accurate power sharing and voltage restoration, with the latter being more significant to the case of parallel converters in a micro-grid architecture. The DC micro-grid consists of multiple DC/DC boost converters, which have nonlinear dynamics, feeding local CPLs, which also exhibit a nonlinear behaviour and introduce negative impedance characteristics that are well-known to yield instability. At the primary control layer, the droop control concept is suitably formulated and implemented using the recently proposed state-limiting PI controller to accomplish an inherent current limitation for each converter and simultaneously facilitate the stability analysis. Using limited information of the injected power from neighbouring converters and, depending on the micro-grid configuration, the load voltage, a distributed secondary controller is formulated to enhance the power sharing and accurately regulate the voltage to the rated value. By analysing for the first time both the dynamics of the converters with the CPLs and the two-layer control, singular perturbation theory is applied to analytically prove the stability of the entire DC micro-grid. The scalability of the system is also ensured through relevant passivity analysis. Simulation and experimental testings are performed to confirm the effectiveness and validity of the proposed method.

Key words: DC micro-grids, constant power loads (CPLs), droop control, distributed control, stability analysis.

1 Introduction

Environmental aspects have urged the conventional power grid to undergo a period of unprecedented change. The replacement of the bulk generation based on synchronous machines, with renewable energy generation units interconnected to the grid via power electronic devices, represents one of the major transitions. Since the majority of renewable generation and storage units run on DC power, DC micro-grids have emerged as a successful solution for integrating them within the future grid. The effects quickly followed with DC micro-grids being implemented in more-electric aircrafts, shipboard systems, data centres, smart communities (Cairoli & Dougal 2013, Buticchi et al. 2017, Salomonsson et al. 2008, Setthapun et al. 2015).

The main challenges in these multiple-source based networks deal with issues related to: i) DC bus voltage maintenance; ii) load power distribution among parallel sources; iii) fault protection; iv) power quality; v) system instability (Jin et al. 2014). Stability of the DC micro-grid continues to remain a challenge due to the nonlinear dynamics that the power electronic converters

and their loads introduce. In particular, DC micro-grids with CPLs tend to be unstable when traditional decentralized control or distributed control strategies are implemented independently. Droop-based methods, formulated in different structures (Shuai et al. 2016, Cingoz et al. 2017, Simpson-Porco et al. 2017, Xu et al. 2015, Jung-Won Kim et al. 2002, Lu et al. 2014, Huang et al. 2015), are most commonly employed to guarantee DC bus voltage regulation, and achieve power sharing. Stability of reduced-order models in droop mode has been investigated in Anand & Fernandes (2013), Tahim et al. (2015) obtaining safe operating ranges for the droop coefficients. Nevertheless, in the majority of these cases, the dynamics of the converters are ignored. Other stability strategies have been developed using the already proposed Brayton and Moser's nonlinear circuit theory (Liu et al. 2011). However, in droop control mode the system suffers from poor voltage regulation, inaccurate load power sharing, slow dynamic response, line impedance dependency, and reduced stability margin (Mohamed & El-Saadany 2008).

To address the load voltage permanent offset and the other shortcomings (e.g. inaccurate power sharing), multi-level or hierarchical control strategies are often adopted as they introduce a certain degree of independence between different control levels and increase the reliability of the system, by continuing to be operational even in case of failures in one of the upper control layers (Gao et al. 2019). In the same framework,

[★] Corresponding author.

Email addresses: a.braitor@sheffield.ac.uk (A.-C. Braitor), g.konstantopoulos@sheffield.ac.uk (G.C. Konstantopoulos), visakan@sheffield.ac.uk (V. Kadiramanathan).

distributed control methods have been proposed in Liu et al. (2018), Zhao & Dörfler (2015), employing a diffusive or nearest-neighbour coupling, where the system and/or the lower control levels dynamics are ignored. The main advantage of these approaches is that the system maintains full functionality, even in case of communication failure of some of the links, given the network remains connected. This is due to the fact that distributed control is immune to single point of failure (SPOF), as shown in Bidram et al. (2013), Shafiee et al. (2014), Loh et al. (2016). Nevertheless, the stability of the micro-grid system, particularly with constant power loads (CPLs), under multi-level distributed control has not been adequately studied, mainly because of the complex dynamics that the hierarchical control, the system and the loads introduce. Hence, the detailed stability of the DC micro-grid system under multi-level distributed control still remains an open problem.

In this paper, the stability analysis of n bidirectional boost converters, which introduce nonlinear dynamics, feeding local CPLs under hierarchical control that guarantees voltage regulation, accurate power sharing and current limitation, is investigated. First, a novel decentralised primary droop control with current limitation is presented motivated by the recently proposed state-limiting PI controller (Konstantopoulos & Baldovino-Monasterios 2019) and by suitably formulating the droop expression. Then, a secondary distributed controller is proposed that ensures accurate power sharing and load voltage restoration. By using a two time-scale analysis approach, stability analysis of the overall system is performed, that includes the dynamics of the DC-DC converters, the CPL and the nonlinear hierarchical control strategy. Simulation and experimental testing are included to verify the proposed control strategy and the theoretical analysis. The key contributions of this paper can be summarized as follows:

- (1) A meshed DC micro-grid architecture with local CPLs is proposed and investigated using graph theory and linear algebra tools. Moreover, the particular case of meshed networks with converters sharing common loads, namely the parallel configuration, is also investigated, as it adds additional challenges into the small-signal analysis due to the singularities introduced by the common CPL into the overall system.
- (2) Compared to Su et al. (2018) in which linear buck converter dynamics are investigated in a parallel micro-grid configuration, in this paper the boost converter dynamics in both meshed and parallel micro-grid architectures are considered, which are inherently nonlinear. Moreover, a new hierarchical control framework is proposed to ensure load voltage restoration and accurate power sharing across the multiple sources, with an inherent input current limitation capability in contrast to Nahata et al. (2020), Han et al. (2019);
- (3) Opposed to Liu et al. (2018) that only investigates

the stability of the secondary controller, and Nahata et al. (2020), Han et al. (2019) that ignore the converter dynamics, in this paper, closed-loop stability is guaranteed, pending straightforward conditions for the entire system, which incorporates the boost converter dynamics, the CPLs and the hierarchical control;

- (4) The DC micro-grid scalability has been demonstrated by investigating the system passivity when plugging in/out an additional converter equipped with the proposed controller.

The paper is organized in the following way. In Section 2, the micro-grid system and the CPL models are put forward. Section 3 describes the novel primary and secondary controllers to achieve tight voltage regulation, accurate load power distribution with the current-limiting capability. Stability of the entire system in both meshed and parallel micro-grid configurations is investigated in Section 4, followed by simulation and experimental testing in Sections 5 and 6, respectively. Finally, conclusions are drawn in Section 7.

The remainder of this section introduces the necessary notations and revisits some key preliminaries.

1.1 Notation and preliminaries

1.1.1 Vectors, matrices and functions

Consider $\mathbf{1}_n$, $\mathbf{1}_{n \times n}$ and $\mathbf{0}_n$, $\mathbf{0}_{n \times n}$ denoting the n -dimensional vector and matrix, of unit and zero entries, respectively, and let $\mathbf{1}_n^\perp$ be the orthogonal complement of $\mathbf{1}_n$ in \mathbb{R}^n , that is, $\mathbf{1}_n^\perp \triangleq \{x \in \mathbb{R}^n : x \perp \mathbf{1}_n\}$. Let I_n be the identity matrix of size n . Given an n -tuple (x_1, \dots, x_n) , let $x \in \mathbb{R}^n$ be the associated vector. For an ordered index set \mathcal{I} of cardinality $|\mathcal{I}|$ and an one-dimensional array $\{x_i\}_{i \in \mathcal{I}}$, we define $[x_i] = \text{diag}(\{x_i\}_{i \in \mathcal{I}}) \in \mathbb{R}^{|\mathcal{I}| \times |\mathcal{I}|}$ to be the associated diagonal matrix. For $x \in \mathbb{R}^n$, define the vector-valued and matrix-valued, respectively, functions $\mathbf{sin}(x) = (\sin(x_1), \dots, \sin(x_n))$, $\mathbf{cos}(x) = (\cos(x_1), \dots, \cos(x_n))$ and $[\mathbf{sin}(x)] = \text{diag}(\{\sin(x_i)\}_{i \in \mathcal{I}})$, $[\mathbf{cos}(x)] = \text{diag}(\{\cos(x_i)\}_{i \in \mathcal{I}})$.

1.1.2 Graph theory

Consider an undirected, connected, and weighted graph $G(\mathcal{V}, \mathcal{E}, A)$, represented as a set of vertices $\mathcal{V} = [\nu_1 \nu_2 \dots \nu_n]$ connected by a set of edges $\mathcal{E} \subset \mathcal{V} \times \mathcal{V}$, and induced by the symmetric, irreducible, and non-negative adjacency matrix $A \in \mathbb{R}^{n \times n}$, with n being the number of vertices. The elements of A represent the weights, where $a_{ij} > 0$ if the edge $(\nu_j, \nu_i) \in \mathcal{E}$, otherwise, $a_{ij} = 0$. The Laplacian matrix $\mathcal{L} \in \mathbb{R}^{n \times n}$ is defined as $\mathcal{L} = [A\mathbf{1}_n] - A$, and its eigenvalues determine the global dynamics. For a connected graph, there is one spanning tree, with $\ker(\mathcal{L}) = \text{span}(\mathbf{1}_n)$, having all $n-1$ remaining eigenvalues of \mathcal{L} real and strictly positive, with the second-smallest eigenvalue $\lambda_2(\mathcal{L})$ called the *algebraic connectivity*.

1.1.3 Linear matrix analysis

Lemma 1 *With $\lambda_1 \leq \lambda_2 \leq \dots \leq \lambda_n$ representing the eigenvalues of a Hermitian matrix A , and $\beta_1 \leq \beta_2 \leq$*

$\dots \leq \beta_n$ the eigenvalues of a Hermitian matrix B , it holds true that

$$\lambda_i + \beta_1 \leq \eta_i \leq \lambda_i + \beta_n$$

where $\eta_1 \leq \eta_2 \leq \dots \leq \eta_n$ are the eigenvalues of the Hermitian matrix $A + B$.

Proof. Presented in Meyer (2000, Ch.7). \square

Lemma 2 Let $Q, R \in \mathbb{C}^{n \times n}$ be two unitary matrices, i.e. $Q^*Q = I_n$ and $R^*R = I_n$, with $*$ denoting the conjugate transpose. Then $P = QR$ is also an unitary matrix.

Proof. By calculating the product P^*P , it is shown that

$$P^*P = (QR)^*QR = R^*(Q^*Q)R = R^*R = I_n$$

which completes the proof. \square

Lemma 3 Let S be a positive-semidefinite Hermitian matrix and D a positive-definite Hermitian matrix. Then

1) Matrix product SD (or DS) is diagonalizable.

2) If $S, D \in \mathbb{R}^{n \times n}$, the eigenvalues of SD (or DS) have only real part, and the product SD (or DS) has the same number of negative (zero, or positive) eigenvalues as matrix A .

Lemma 4 Let \mathcal{L} be the Laplacian matrix of a connected and undirected graph \mathcal{G} with n vertices, and a vector $y \in \mathbb{R}_{\geq 0}^n$, with $y \neq \mathbf{0}_n$, such that $\Delta = \text{diag}\{y\}$. By considering the Laplacian matrix

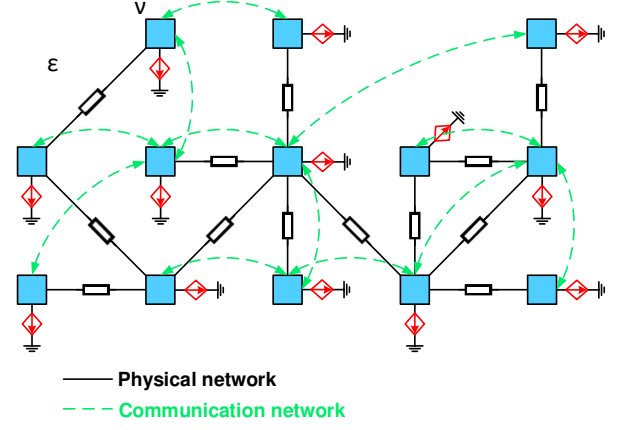
$$\mathcal{L}^\dagger = \begin{bmatrix} y^T y & -y^T \\ -y & \mathcal{L} + \Delta \end{bmatrix}$$

corresponding to a graph \mathcal{G}^\dagger , one can conclude that matrix $\mathcal{L} + \Delta$ is positive-definite.

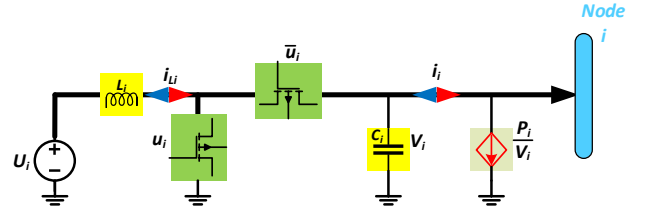
2 Dynamic modelling of a DC Micro-grid

A typical islanded DC micro-grid is depicted in Fig. 1a, consisting of n nodes, representing bidirectional DC/DC boost converters (Fig. 1b), connected in a meshed configuration, feeding local loads (CPLs). Every converter includes a boosting inductor L_i , a smoothing capacitor C_i , while U_i is the DC input voltage, where $i \in \mathcal{I}$. One can also see, the mapping of the cyber network, which can be different to the physical network, onto the physical DC micro-grid. The vertices represent converter nodes, and the edges represent the communication links for information exchange. In achieving global synchronization, the communication graph must have at least one spanning tree. Hence the communication network is represented by an undirected, connected and unweighted graph, and the inertia of its Laplacian matrix \mathcal{L}_{cyb} , is $i(\mathcal{L}_{cyb}) = [n-1 \ 0 \ 1]$. Diffusive coupling (nearest-neighbour coupling) is the most common type of coupling in distributed communication networks.

The system's nonlinear dynamic model can be described by employing Kirchhoff laws and average analysis (Ortega et al. 1998), leading to the following differential equations:



(a) Typical framework of a meshed DC micro-grid



(b) Power converter integration into the network

Fig. 1. The structure of the DC micro-grid system

$$L_i \dot{i}_{L_i} = U_i - (1 - u_i)V_i \quad (1)$$

$$C_i \dot{V}_i = (1 - u_i)i_{L_i} - i_i \quad (2)$$

where u_i is the duty-ratio (control) input, bounded in the range $[0, 1]$, i_{L_i} is the inductor current and V_i, i_i are the converter output voltage and current, respectively.

Rewriting (1)-(2) in a matrix form, the DC micro-grid system takes the following form

$$\dot{i}_L = L^{-1}(U - (I_n - u)V) \quad (3)$$

$$\dot{V} = C^{-1}((I_n - u)i_L - i) \quad (4)$$

where $U = [U_1 \dots U_n]^T$, $u = \text{diag}\{u_i\}$, $V = [V_1 \dots V_n]^T$, $i_L = [i_{L1} \dots i_{Ln}]^T$, $i = [i_1 \dots i_n]^T$, $L = \text{diag}\{L_i\}$ and $C = \text{diag}\{C_i\}$. It is clear that system (3)-(4) is nonlinear, since the control input u is multiplied with the system states $\begin{bmatrix} i_L^T & V^T \end{bmatrix}^T$.

One can write the output current of each converter as

$$i_i = \frac{P_i}{V_i} + \sum_{k \in \mathcal{N}_i} i_{ik}, \quad (5)$$

where P_i is constant and represents the local power demand in node i , while \mathcal{N}_i represents the neighbourhood of node i , in the induced graph described by the meshed DC network, i.e. $\mathcal{N}_i \in \mathcal{V} : \varepsilon_{ik} \in \mathcal{E}$.

Considering a steady-state voltage value for the i -th node denoted by V_{ie} , by taking the partial derivative of output current i_i from (5) with respect to the output voltage V_i , one obtains the conductance matrix

$$Y = \mathcal{L} - D, \quad (6)$$

where \mathcal{L} is a positive semi-definite and $D = \text{diag}\{\frac{P_i}{V_i^2}\}$ a positive-definite matrix. Note that the symmetric matrix \mathcal{L} represents the Laplacian matrix induced by the DC network, while the diagonal matrix D incorporates the self-loops of the nodes.

2.1 Common load micro-grid topology

A special case of the meshed architecture, that introduces the challenges of load voltage regulation and power sharing, is the parallel configuration. Therein, the power balance equation for the CPL becomes $P = V_o \sum_{i=1}^n i_i$, with constant P representing the common load power demand, and V_o being the load voltage. The output currents expression would then be given as $i_i = \frac{V_i - V_o}{R_i}$. Similar to Simpson-Porco et al. (2017), Su et al. (2018), Liu et al. (2018) and by following the theoretical proof developed in Braiton et al. (2020a,c), the feasible solution of the load voltage V_o becomes

$$V_o = \frac{\sum_{i=1}^n \frac{V_i}{R_i} + \sqrt{\left(\sum_{i=1}^n \frac{V_i}{R_i}\right)^2 - 4P \sum_{i=1}^n \frac{1}{R_i}}}{2 \sum_{i=1}^n \frac{1}{R_i}}. \quad (7)$$

It should be underlined that theoretically, there are two possible expressions for the load voltage, a high and a low voltage. However, if a current-limiting property $|i_{Li}| \leq |i_{Li}^{max}|$ is guaranteed, then not only each converter is inherently protected, but also as shown in Braiton et al. (2020a,c), only the high load voltage solution is possible. This can be accomplished with the proposed controller as it will be explained in the sequel.

Remark 1 Note that compared to Simpson-Porco et al. (2017), Su et al. (2018), Liu et al. (2018) that assume the load voltage given as in equation (7) based on the feasibility of the high-voltage solution, in this work it can be analytically guaranteed through the current-limiting property of the proposed controller.

Obviously, the existence of a real solution of the load voltage requires the expression in the square root in (7) to be non-negative. Hence, for higher values of the load power P , the output voltages of the converters should be increased or a higher rated voltage of the DC micro-grid can be considered, as discussed in Su et al. (2018).

For an equilibrium point (i_{Lie}, V_{ie}) given by a constant control input u_i , by taking the partial derivative of the output current $i_i = \frac{V_i - V_o}{R_i}$ with respect to the output voltage V_i , as in Braiton et al. (2020a,c), Braiton et al. (2020b) we obtain the conductance matrix, in parallel configuration case, as

$$Y = R^{-1} (I_n - \mathbf{1}_{n \times n} D), \quad (8)$$

with $R = \text{diag}\{R_i\}$ and $D = \text{diag}\{\frac{\partial V_i}{\partial V_o}\} > 0, \forall i \in \mathcal{I}$. For a more thorough explanation and in-depth expansion of the conductance matrix for parallel configuration micro-grids with CPL, the reader is referred to Braiton et al. (2020b).

3 Proposed controller design

3.1 Primary control steady-state analysis

The key grid-forming control strategy in modern micro-grids, consisting of multiple distributed generation units, is represented by the well-established droop control, which in its conventional dynamic form is

$$\tau_i \dot{V}_i = V^* - V_i - m_i P_{inj,i}. \quad (9)$$

where $P_{inj,i}$ is the injected power by the i -th converter, V^* is the rated/nominal voltage, τ_i is the time-constant, and m_i is the positive droop coefficient chosen to satisfy

$$m_i \leq \frac{V^*}{P_i}. \quad (10)$$

By further looking into (9), it is clear that the output voltage V_i will deviate from the nominal voltage V^* as long as $P_{inj,i} \neq 0$. Furthermore, the larger the droop gain m_i , the more the voltage deviation $V^* - V_i$ becomes.

In order to regulate the output voltage V_i to the nominal value V^* , and at the same time maintain the power sharing accuracy, a correction term, e_i is added into the droop function (9), as

$$\tau_i \dot{V}_i = V^* - V_i - m_i P_{inj,i} + e_i, \quad (11)$$

where e_i is obtained from the dynamics of the secondary control layer. The first task of this paper is to design a primary controller that inherits the droop control concept and additionally maintains an upper limitation for the input current for each converter independently of the system parameters. To this end, the duty-ratio input of each boost converter is proposed to take the form

$$u_i = 1 - \frac{r_{vi} i_{Li} + U_i - E_{maxi} \sin \sigma_i}{V_i}, \quad (12)$$

where r_{vi} represents a constant virtual resistance and E_{maxi} a constant maximum virtual voltage for the i -th converter, chosen to satisfy, in matrix form, $I_{max} = E_{max} r_v^{-1}$. Inspired by the state-limiting PI (sl-PI) controller proposed in Konstantopoulos & Baldivieso-Monasterios (2019), σ_i is designed to follow the nonlinear dynamics:

$$\dot{\sigma}_i = \frac{k_i}{E_{maxi}} \left(V^* - V_i - m_i \frac{U_i E_{maxi} \sin \sigma_i}{r_{vi}} + e_i \right) \cos \sigma_i \quad (13)$$

with k_i, E_{maxi} being positive constants and $\sigma_i(0) = 0$.

Proposition 1 The controller state $\sigma_i(t)$ is uniformly ultimately bounded, within the range $\sigma_i \in [-\frac{\pi}{2}, \frac{\pi}{2}]$.

Proof. Based on the sl-PI properties given in Konstantopoulos & Baldivieso-Monasterios (2019). \square

A detailed diagram of the control implementation is shown in Fig. 2. Note that the droop function in the proposed control dynamics (13) differs from the conventional one in (11), since the term $P_{inj,i}$ has been replaced with $\frac{U_i E_{maxi} \sin \sigma_i}{r_{vi}}$. In order to explain why the new term represents the converter power at the steady-state, let us replace the control input, u_i , from (12) into (1). This results in the closed-loop current dynamics

$$L_i \dot{i}_{Li} = -r_{vi} i_{Li} + E_{maxi} \sin \sigma_i, \quad (14)$$

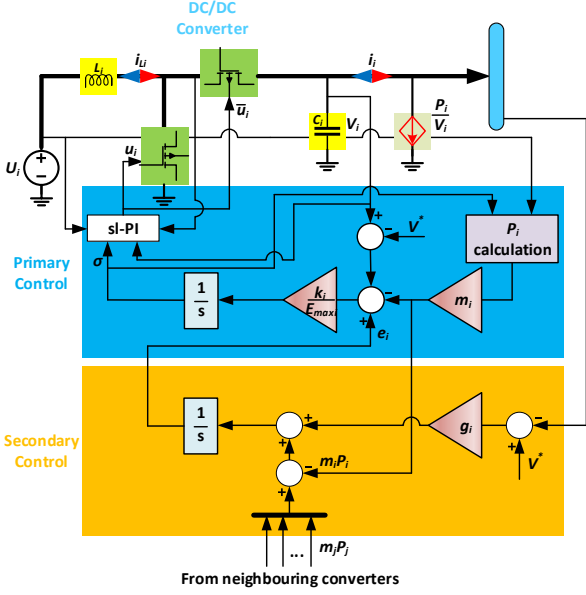


Fig. 2. Detailed diagram with primary and secondary controller

where one can observe that $E_{maxi} \sin \sigma_i$ represents a virtual voltage, and r_{vi} a virtual resistance. At steady state there is

$$i_{Li} = \frac{E_{maxi} \sin \sigma_i}{r_{vi}}, \quad (15)$$

and since $P_{inj,i} = U_i i_{Li}$, equation (13) has incorporated the expression

$$P_{inj,i} \approx \frac{U_i E_{maxi} \sin \sigma_i}{r_{vi}}, \quad (16)$$

which will represent the converter power at steady state.

Proposition 2 *The solution $i_{Li}(t)$ of (14) is uniformly ultimately bounded, i.e. $|i_{Li}(t)| \leq i_{Li}^{max}, \forall t \geq 0$, with the maximum current given as $i_{Li}^{max} = \frac{E_{maxi}}{r_{vi}}$.*

Proof. Following a similar approach as in Braitor et al. (2020a,c). \square

This new primary control structure has been proposed to facilitate the stability analysis of the entire micro-grid, as it will be further explained in Section 4.

3.2 Secondary control design and analysis

The second task herein is to design a secondary controller that meets the power sharing requirements,

$$\lim_{t \rightarrow \infty} \sum_{j \in \mathcal{N}_i} (m_j P_{inj,j}(t) - m_i P_{inj,i}(t)) = 0 \quad (17)$$

where $\mathcal{N}_i \subset \mathcal{V} : (\nu_j, \nu_i) \in \mathcal{E}$ denotes the neighbourhood set of the i -th vertex of the cyber network. Furthermore in the parallel operation case, DC bus voltage restoration to the rated value V^* is additionally required, i.e.,

$$\lim_{t \rightarrow \infty} (V^* - V_o)(t) = 0. \quad (18)$$

Then the distributed secondary control that generates the correction term e_i for the primary controller can be designed in the dynamic form

$$\dot{e}_i = \alpha g_i (V^* - V_o) + \beta \sum_{j \in \mathcal{N}_i} (m_j P_{inj,j} - m_i P_{inj,i}) \quad (19)$$

where $\alpha, \beta \in \mathbb{R}^+$ are constant gains, $g_i = \{0, 1\}$, and P_i, P_j given from (16). Note that in meshed configurations where there are no shared loads, the control gain $\alpha = 0$. Driven by the concept of the pinning control, since the DC bus voltage V_o may not be known by all the DGs, the pinning gain g_i is introduced, being non-zero for the DG that has access to the DC bus voltage V_o . By applying the secondary controller at each converter, (19) can be written in the matrix form

$$\dot{e} = \alpha g (V^* - V_o) \mathbf{1}_n - \beta \mathcal{L}_{cyb} m P_{inj} \quad (20)$$

where $g = \text{diag}\{g_i\}$, $m = \text{diag}\{m_i\}$, and $P_{inj} = [P_{inj,1} \dots P_{inj,n}]$. At the steady state there is

$$\alpha g (V^* - V_o) \mathbf{1}_n - \beta \mathcal{L}_{cyb} m P_{inj} = \mathbf{0}_n \quad (21)$$

Corollary 1 *Since $m_i \neq 0$ and assuming that at least one converter measures the load voltage, i.e. $\sum_{i=1}^n g_i > 0$, the following equations hold:*

$$m_1 P_{inj,1} = m_2 P_{inj,2} = \dots = m_n P_{inj,n} \quad (22)$$

$$V_o = V^*. \quad (23)$$

Remark 2 *One can clearly notice that in the case of meshed architectures, where the voltage restoration term of equation (20) disappears, the proof is more straightforward than the one presented for Corollary 1 in Appendix C. Since the cyber network induces a connected, undirected and balanced graph, its corresponding Laplacian matrix \mathcal{L}_{cyb} guarantees that equality (22) holds at the steady state.*

4 Stability Analysis

4.1 Closed-loop system

By applying the proposed controller (12)-(13), (19) into the DC micro-grid dynamics (1)-(2), the closed-loop system can be written in the following matrix form

$$\begin{bmatrix} \dot{i}_L \\ \dot{V} \end{bmatrix} = \begin{bmatrix} L^{-1} (-r_v i_L + E_{max} \mathbf{sin}(\sigma)) \\ C^{-1} [V]^{-1} (r_v [i_L] + [U] - E_{max} [\mathbf{sin}(\sigma)]) i_L - i \end{bmatrix} \quad (24)$$

$$\begin{bmatrix} \dot{\sigma} \\ \dot{e} \end{bmatrix} = \begin{bmatrix} E_{max}^{-1} k [\mathbf{cos}(\sigma)] (V^* - V - [r_v]^{-1} m [U] E_{max} \mathbf{sin}(\sigma) + e) \\ \alpha g (V^* - V_o) \mathbf{1}_n - \beta \mathcal{L}_{cyb} m P_{inj} \end{bmatrix} \quad (25)$$

where $\sigma = [\sigma_1 \dots \sigma_n]^T$, $k = \text{diag}\{k_i\}$, $E_{max} = \text{diag}\{E_{maxi}\}$. For the closed-loop system, consider the following assumption:

Assumption 1 *For a constant $\sigma_{ie} \in (-\frac{\pi}{2}, \frac{\pi}{2})$, satisfying (22), there exists a unique equilibrium point $(i_{Lie}, V_{ie}, \sigma_{ie}, e_{ie})$, corresponding to the desired voltage regulation (23).*

The above assumption is considered since the proof of the existence of a unique equilibrium point for a micro-grid with primary and secondary control is a non-trivial

problem, as one can see from Simpson-Porco et al. (2017), Liu et al. (2018).

Since r_{vi} and k_i represent control parameters, they can be suitably selected in order for the terms $\frac{L_i}{r_{vi}}$ and $\frac{1}{k_i}$ to be sufficiently small. Hence, by introducing the perturbation parameter ε , as $\varepsilon = \min\{\frac{1}{k_i}, \frac{L_i}{r_{vi}}\}$, one can conclude that there exist $\delta_L = \text{diag}\{\delta_{Li}\} \geq 0$ and $\delta_\sigma = \text{diag}\{\delta_{\sigma i}\} \geq 0$ such that $Lr_v^{-1} = \frac{1}{\varepsilon}I_n + \delta_L$ and $k = \frac{1}{\varepsilon}I_n + \delta_\sigma$. Hence, (25) becomes as shown in (26), where it has been taken into account that $I_{max} = r_v^{-1}E_{max}$. Therefore, the closed-loop system equations (24) and (25) can be written in the following form

$$\dot{x} = f(x, z) \quad (27)$$

$$\varepsilon \dot{z} = q(x, z, \varepsilon) \quad (28)$$

where $x = \begin{bmatrix} V - V_e \\ e - e_e \end{bmatrix}$ and $z = \begin{bmatrix} i_L - i_{Le} \\ \sigma - \sigma_e \end{bmatrix}$. System (27)-

(28) can then be investigated as a singularly perturbed system using two-time-scale analysis (H.K.Khalil 2014). Since it represents the immediate vicinity of a bounding surface, system (26) is also referred to as the boundary layer, and it is analyzed in the section below.

4.2 Boundary layer stability analysis

Let functions f, q be continuously differentiable in the domain $(x, z, \varepsilon) \in D_x \times D_z \times [0, \varepsilon_0]$. Considering the scenario where the controller parameters r_{vi} and k_i are selected sufficiently large, then $\varepsilon \rightarrow 0$ and, according to the singular perturbation theory, function q will have an algebraic form of $0 = q(x, z)$ as follows

$$\mathbf{0}_{2n} = \begin{bmatrix} -i_L + I_{max} \mathbf{sin}(\sigma) \\ E_{max}^{-1} [\mathbf{cos}(\sigma)] (V^* - V - m[U] I_{max} \mathbf{sin}(\sigma) + e) \end{bmatrix}$$

The roots of the above system can be computed as

$$\begin{bmatrix} i_L \\ \sigma \end{bmatrix} = \begin{bmatrix} I_{max} \mathbf{sin}(\sigma) \\ \mathbf{sin}^{-1}(m^{-1}[U]^{-1} I_{max}^{-1} (V^* I_n - [V] + [e])) \end{bmatrix} \quad (29)$$

and can also be referred to as $z = h(x)$ with $\sigma_i \in (-\frac{\pi}{2}, \frac{\pi}{2})$, such that $h(0) = 0$. Thus, the roots also represent the equilibrium points of the nonlinear system (24)-(25). Exponential stability at the origin can be investigated via its corresponding Jacobian matrix:

$$J_1 = \begin{bmatrix} -I_n & I_{max} [\mathbf{cos}(\sigma)] \\ \mathbf{0}_{n \times n} & -[\mathbf{cos}(\sigma)]^2 E_{max}^{-1} m[U] I_{max} \end{bmatrix}. \quad (30)$$

As one can observe matrix J_1 is Hurwitz, since J_1 is upper triangular and all its diagonal elements are negative. Hence, there exist $\rho_1 > 0$ and a domain $\tilde{D}_z = \{z \in R^{2n}, \|z\|_2 < \rho_1\}$ where $\tilde{D}_z \subseteq D_z$ such that (28) is exponentially stable at the origin uniformly in x .

4.3 Reduced model

To obtain the reduced model, the roots i_L and σ are substituted from (29) into (24)-(25), yielding

$$\dot{V} = C^{-1} [V]^{-1} m^{-1} (V^* \mathbf{1}_n - V - e) - C^{-1} i \quad (31)$$

$$\dot{e} = \alpha g (V^* - V_o) \mathbf{1}_n - \beta \mathcal{L}_{cyb} (V^* \mathbf{1}_n - V + e) \quad (32)$$

often referred to as the quasi-steady-state model, because i_L , and σ , introduce a velocity $[\dot{i}_L \dot{\sigma}]^T = \varepsilon^{-1} q$ which is very large when ε is small and $q \neq 0$. This leads to rapid convergence to a root $h(V, e)$, which is also the equilibrium of the boundary-layer. The stability analysis of the reduced-order model follows different proofs depending on the micro-grid configuration, which not only induces distinct network graphs with different adopted expressions of the conductance matrices, but also influences the secondary control design by excluding the voltage restoration term. Hence, the meshed and parallel micro-grid configuration cases will be investigated separately in the reduced-order model.

The corresponding Jacobian J_2 of the reduced model (31)-(32) becomes as shown in (33).

4.3.1 Meshed micro-grid configuration

In the generic meshed architecture, the load voltage restoration term is not needed as the converters do not share any load, thus the control gain $\alpha = 0$. By substituting the conductance matrix with its expression from (6), the Jacobian matrix J_2 can be rewritten as $J_{2, \alpha=0} = -\beta J_3 + Q_1$, with

$$J_3 = \underbrace{\begin{bmatrix} \frac{1}{\beta} C^{-1} [V_e]^{-1} m^{-1} \mathbf{0}_{n \times n} \\ \mathbf{0}_{n \times n} & \mathcal{L}_{cyb} \end{bmatrix}}_{X_1} \underbrace{\begin{bmatrix} [V_e]^{-1} (V^* I_n + [e]) + [V_e] m \mathcal{L} & -I_n \\ -I_n & I_n \end{bmatrix}}_{X_2},$$

and

$$Q_1 = \begin{bmatrix} C^{-1} D \mathbf{0}_{n \times n} \\ \mathbf{0}_{n \times n} & \mathbf{0}_{n \times n} \end{bmatrix}.$$

One notices that the block-diagonal matrices Q_1 and X_1 are positive semi-definite, the latter having $\mathcal{L}_{cyb} \succeq 0$ on its main diagonal. Consider the following lemma.

Lemma 5 *Matrix $X_1 X_2$ (or $X_2 X_1$) is semi-positive stable and diagonalizable.*

One can write the standard eigenvalue problem (SEP) for the Jacobian matrix $J_{2, \alpha=2}$ as

$$(-\beta X_1 X_2 + Q_1) \bar{x} = \lambda \bar{x}. \quad (34)$$

where $\lambda \in \mathbb{R}$ is an eigenvalue and $\bar{x} \in \mathbb{R}^n$ is the associated eigenvector. As $X_2 \succ 0$ (Lemma 5), by taking the similarity transformation $\bar{J}_{2, \alpha=0} = X_2 J_{2, \alpha=0} X_2^{-1}$, one gets

$$\left(-\beta \underbrace{X_2 X_1}_{\bar{J}_3} + \underbrace{X_2 Q_1 X_2^{-1}}_{\bar{Q}_1} \right) \bar{v} = \lambda \bar{v}. \quad (35)$$

$$\begin{bmatrix} \varepsilon \dot{i}_L \\ \varepsilon \dot{\sigma} \end{bmatrix} = \begin{bmatrix} (I_n + \varepsilon \delta_L) (-i_L + I_{max} \mathbf{sin}(\sigma)) \\ (I_n + \varepsilon \delta_\sigma) E_{max}^{-1} [\mathbf{cos}(\sigma)] (V^* - V - m [U] I_{max} \mathbf{sin}(\sigma) + e) \end{bmatrix} \quad (26)$$

$$J_2 = \begin{bmatrix} -C^{-1} [V_e]^{-2} m^{-1} (V^* I_n + [e]) - C^{-1} Y C^{-1} [V_e]^{-1} m^{-1} \\ -\alpha g \mathbf{1}_{n \times n} D + \beta \mathcal{L}_{cyb} & -\beta \mathcal{L}_{cyb} \end{bmatrix} \quad (33)$$

Theorem 1 The equilibrium point $(i_{Lie}, V_{ie}, \sigma_{ie}, e_{ie})$ of the reduced system (31)-(32), when $\alpha = 0$, is exponentially stable if

$$\beta > \max \left\{ P_i \left(C_i V_i^2 \min_{\bar{z}^T \bar{z} \neq 0} \frac{\bar{z}^T \Lambda_1 \bar{z}}{\bar{z}^T \bar{z}} \right)^{-1} \right\}, \forall i \in \mathcal{I}. \quad (36)$$

where Λ_1 is diagonal with same index of inertia as $X_2 X_1$. By virtue of H.K.Khalil (2014, Th.11.4), there exists $\varepsilon^* = \min\{\frac{\min\{L_i\}}{r_v^*}, \frac{1}{k^*} > 0\}$ such that for all $\varepsilon < \varepsilon^*$ (or equivalently $\frac{r_{vi}}{L_i} > \frac{r_v^*}{\min\{L_i\}}$, or $k_i > k^*$), the equilibrium point $[i_{Le}^T V_e^T \sigma_e^T e_e^T]^T$ of (27)-(28) with $\sigma_{ie} \in (-\frac{\pi}{2}, \frac{\pi}{2})$ is exponentially stable. This concludes the stability analysis of the generic meshed DC micro-grid.

A special case of meshed micro-grids where converters share the same load and the voltage restoration term would make sense, thus $\alpha \neq 0$, is the parallel configuration case which is investigated next.

4.3.2 Parallel micro-grid configuration

The Jacobian matrix J_2 can be rewritten as a sum of two matrices, i.e., $J_{2,\alpha \neq 0} = \alpha J_4 - \beta J_5$, with

$$J_4 = \underbrace{\begin{bmatrix} \frac{1}{\alpha} C^{-1} R^{-1} & -g \\ -g & \frac{1}{\alpha} I_n \end{bmatrix}}_{X_3} \underbrace{\begin{bmatrix} \mathbf{1}_{n \times n} & \mathbf{0}_{n \times n} \\ \mathbf{0}_{n \times n} & \mathbf{0}_{n \times n} \end{bmatrix}}_{X_4} \underbrace{\begin{bmatrix} D & \mathbf{0}_{n \times n} \\ \mathbf{0}_{n \times n} & D \end{bmatrix}}_{Q_2}$$

and

$$J_5 = X_1 \times \underbrace{\begin{bmatrix} [V_e]^{-1} (V^* I_n + [e]) + [V_e] m R^{-1} & -I_n \\ -I_n & I_n \end{bmatrix}}_{X_5}.$$

Hence, the stability problem becomes an SEP, i.e. $J_{2,\alpha \neq 0} \bar{y} = \lambda \bar{y}$, which gives

$$(\alpha X_3 X_4 Q_2 - \beta X_1 X_5) \bar{y} = \lambda \bar{y} \quad (37)$$

where $\lambda \in \mathbb{R}$ is an eigenvalue and $\bar{y} \in \mathbb{R}^n$ is the associated eigenvector. Let $\bar{w} \triangleq Q_2 \bar{y}$; then the SEP becomes $\bar{J}_{2,\alpha \neq 0} \bar{w} = \lambda \bar{w}$, as follows

$$\left(\alpha \underbrace{X_3 X_4}_{\bar{J}_4} - \beta \underbrace{X_1 X_5 Q_2^{-1}}_{\bar{J}_5} \right) \bar{w} = \lambda \bar{w} \quad (38)$$

Lemma 6 Matrix $\bar{J}_4 = X_3 X_4$ is semi-positive stable and diagonalizable if

$$\alpha < \frac{1}{C_i^{\frac{1}{4}} R_i^{\frac{1}{4}}}, \forall i \in \mathcal{I}, \quad (39)$$

where the pinning control gain $g_i = 1$.

Lemma 7 Matrix $\bar{J}_5 = X_1 X_5 Q_2^{-1}$ is diagonalizable and semi-positive stable.

Now, let the following similarity transformation $\tilde{J}_{2,\alpha \neq 0} = (X_5 Q_2^{-1}) \bar{J}_{2,\alpha \neq 0} (Q_2 X_5^{-1})$ for the SEP (38). Hence

$$X_5 Q_2^{-1} (\alpha \bar{J}_4 - \beta \bar{J}_5) Q_2 X_5^{-1} \bar{u} = \lambda \bar{u} \quad (40)$$

which gives

$$\left(\alpha \underbrace{X_5 Q_2^{-1} \bar{J}_4 Q_2 X_5^{-1}}_{\tilde{J}_4} - \beta \underbrace{X_5 Q_2^{-1} X_1}_{\tilde{J}_5} \right) \bar{u} = \lambda \bar{u} \quad (41)$$

Remark 3 According to Sylvester's Law of inertia, the similar matrices $J_{2,\alpha \neq 0}$, $\bar{J}_{2,\alpha \neq 0}$ and $\tilde{J}_{2,\alpha \neq 0}$ have the same inertia, i.e. same number of positive, negative and null eigenvalues.

Theorem 2 The equilibrium point $(i_{Lie}, V_{ie}, \sigma_{ie}, e_{ie})$ of the reduced system (31)-(32), when $\alpha \neq 0$, is exponentially stable if (39) is satisfied and

$$\beta > \frac{\sum_{i=1}^n \frac{1}{C_i R_i}}{\min_{\bar{u}^T \bar{u} \neq 0} \frac{\bar{u}^T \Lambda_2 \bar{u}}{\bar{u}^T \bar{u}}}, \forall i \in \mathcal{I} \quad (42)$$

holds, where Λ_2 is diagonal having the same index of inertia as matrix \bar{J}_4 .

According to H.K.Khalil (2014, Th.11.4), there exists $\varepsilon^* = \min\{\frac{\min\{L_i\}}{r_v^*}, \frac{1}{k^*} > 0\}$ such that for all $\varepsilon < \varepsilon^*$ (or equivalently $\frac{r_{vi}}{L_i} > \frac{r_v^*}{\min\{L_i\}}$, or $k_i > k^*$), the equilibrium point $[i_{Le}^T V_e^T \sigma_e^T e_e^T]^T$ of (27)-(28) with $\sigma_{ie} \in (-\frac{\pi}{2}, \frac{\pi}{2})$ is exponentially stable; thus completing the stability analysis of the entire parallel DC micro-grid architecture.

Remark 4 Note that the presence of a parasitic resistance r_s in series with the converter inductor would not affect the stability result, due to the additional damping introduced into the converter current dynamics. Nonetheless, one can consider the following control law

$$u = 1 - \frac{(r_{vi} + r_s) i_{Li} + U_i - E_{maxi} \sin \sigma_i}{V_i}$$

instead of (12), and result in the same stability analysis.

It is worth mentioning, at this point, that the impact of time delays, which may occur in the secondary control implementation, on the stability of the entire micro-grid is of great interest, see Milano & Anghel (2012), Coelho et al. (2016). In particular, several methods for computing the maximum delay to avoid instability, such as Pade approximations (Jr. & Graves-Morris 1996) or by using Rekasius substitution-based algorithm (Jia et al. 2007), have been designed. In the same framework, Lyapunov-based methods (Polyakov et al. 2015), such as the Implicit Lyapunov Krasovski Functional (ILKF) have emerged to provide sufficient stability conditions. Nevertheless, the main aim of this paper was to introduce for the first time this novel two-level control for the nonlinear model of the DC micro-grid with multiple nonlinear boost converters and guarantee its stability. Future research will focus on investigating the effect of delays to this particular design.

4.4 Micro-grid scalability

In order to guarantee the system scalability, i.e. if one converter, for instance, is plugged in/out, the passivity property of the system with the primary controller needs to be investigated. Let the input $u = V_{n+1} - V_{n+1,e}$, and the output $y = i_{n+1}$, being the output voltage and current, respectively, of the $n+1$ converter. The network structure changes, and the output current vector of the micro-grid system with n converters becomes

$$\dot{i} = Y' \begin{bmatrix} \tilde{V}_1 \\ \vdots \\ u \end{bmatrix} = \underbrace{(\mathcal{L}' - D')}_{\gamma} \tilde{V} + \begin{bmatrix} \frac{\partial i_1}{\partial u} \\ \vdots \\ \frac{\partial i_n}{\partial u} \end{bmatrix} u$$

where $\tilde{V} = V - V_e$ is the shifted state to the origin.

Remark 5 Note that for the parallel micro-grid configuration case, one considers the input $u = V_{n+1} - V_{oe}$. Then, the output current vector of the micro-grid system with n converters becomes

$$\dot{i} = Y' \begin{bmatrix} \tilde{V}_1 \\ \vdots \\ u \end{bmatrix} = \underbrace{R^{-1} (I_n - \mathbf{1}_n \times_n D')}_{\gamma} \tilde{V} + R^{-1} \begin{pmatrix} \frac{\partial \tilde{V}_o}{\partial u} \\ \vdots \\ \frac{\partial \tilde{V}_o}{\partial u} \end{pmatrix} u$$

where $\tilde{V}_o = V_o - V_{oe}$, having with the following expression

$$\tilde{V}_o = \begin{bmatrix} \frac{\partial \tilde{V}_o}{\partial \tilde{V}_1} & \dots & \frac{\partial \tilde{V}_o}{\partial \tilde{V}_n} \end{bmatrix} \tilde{V} + \frac{\partial \tilde{V}_o}{\partial u} u.$$

Next, consider the vector state $x = \begin{bmatrix} x_1^T & x_2^T & x_3^T \end{bmatrix}^T$, with $x_1 = i_L - i_{Le}$, $x_2 = V - V_e$, and $x_3 = \sigma - \sigma_e$. One can write the plant system as

$$\dot{x} = \bar{A}x + \bar{B}u \quad (43)$$

$$y = \bar{C}x + \bar{D}u \quad (44)$$

with the scalar $\bar{D} = -\sum_{k \in \mathcal{N}_{n+1}} \frac{1}{R_k} + \frac{P_{n+1}}{V_{n+1}^2} < 0$ (or $\bar{D} = \frac{1}{R_{n+1}} \left(\frac{\partial \tilde{V}_o}{\partial u} - 1 \right) < 0$ for the parallel micro-grid configuration case). Conducting the same time-scale separation approach as in Section 4.3, one can obtain the boundary layer system with a similar Jacobian matrix as matrix J_1 , which is upper triangular, with the diagonal elements being negative-definite diagonal matrices, therefore, Hurwitz. The roots of the boundary layer system have the same expression as in (29). Hence, the reduced system can be obtained, whose corresponding Jacobian matrix has the form

$$J_2' = -C^{-1} [V_e]^{-2} m^{-1} (V^* I_{n+1} + [e]) - C^{-1} \gamma \quad (45)$$

with $\gamma = \mathcal{L}' + D'$, and $\mathcal{L}' \succ 0$ according to Lemma 4. By Lemma 1, Matrix J_2' is Hurwitz if the following sufficient condition in scalar form

$$\frac{V^* + e_{ie}}{m_i V_{ie}^2} + \min\{\lambda_{\mathcal{L},i}\} - \frac{P_i}{V_{ie}^2} > 0 \quad (46)$$

holds. The above condition is always satisfied by appropriately selecting m_i as specified in equation (10). Note that for parallel topology, $\gamma \succ 0$ by virtue of Lemma 4, in which case J_2' is Hurwitz, as both terms of the sum are negative definite matrices. Thus, according to H.K.Khalil (2014, Th.11.4), the system is exponentially stable. Thus matrix \bar{A} is Hurwitz, hence, there exists a matrix $P = P^T \succ 0$, such that $\bar{A}^T P + P \bar{A} \prec 0$. Then, based on Xia et al. (2015, Th.1) the system is passive if the following inequality given by the Schur complement

$$\left(\bar{A}^T P + P \bar{A} \right) + \left(P \bar{B} - \bar{C}^T \right) \left(\bar{D}^T + \bar{D} \right)^{-1} \left(\bar{B}^T P - \bar{C} \right) \prec 0 \quad (47)$$

holds. The negative scalar $\left(\bar{D}^T + \bar{D} \right)^{-1}$ can be moved in front of the expression and, hence, be multiplied by a term that has the form $v^T v \succeq 0$, where $v = \bar{B}^T P - \bar{C}$. Therefore, the second term of the inequality is negative semi-definite. Since both terms are Hermitian, one being strictly negative definite, and the other is negative semi-definite, their sum is always strictly negative definite, satisfying (47). Thus, the passivity of the plant system can be proven according to Xia et al. (2015, Th.1).

Although the passivity property of the system is important to illustrate the scalability of the micro-grid, it remains an input-output property. Hence, the stability analysis presented in Section 4.3 should be considered to ensure the stable operation of the micro-grid with a generic number of n converters.

5 Simulation results

To test the theoretical findings, simulations are being performed in Matlab/Simulink. The two DC micro-

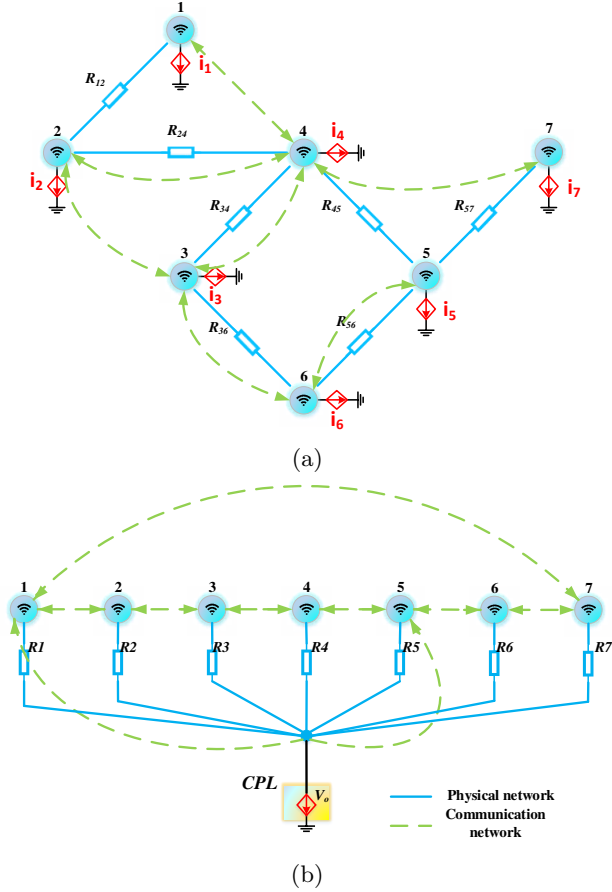


Fig. 3. DC micro-grid example consisting of 7 converters in (a) meshed topology, with local CPLs, each of them communicating with their respective neighbours and (b) parallel configuration, feeding a common CPL, with converters 1 and 5 sampling the load voltage and participating in the voltage restoration

grid configurations considered for testing are presented in Fig. 3, with the parameters specified in Table 1, both topologies consisting of the same seven converters. Each source is driven by bidirectional boost converters connected to local CPLs in the meshed architecture, or to a common CPL in the parallel configuration. The rated voltage is set to $V^* = 400\text{ V}$.

5.1 Meshed micro-grid topology case

One can see in Fig. 3a, the meshed DC micro-grid configuration with the line impedances being $R_{12} = 1.4\ \Omega$, $R_{24} = 1.8\ \Omega$, $R_{34} = 1.1\ \Omega$, $R_{45} = 2.2\ \Omega$, $R_{36} = 1.9\ \Omega$, $R_{56} = 0.5\ \Omega$, $R_{57} = 1.5\ \Omega$. Note that the physical and communication architecture describe different network graphs. The aim is to regulate the converters output voltage close to the rated value based on the droop control concept, and ensure that the sources inject power into the network to satisfy the $7 : 6 : 5 : 4 : 3 : 2 : 1$ imposed agreement, while guaranteeing the current limitation of individual units.

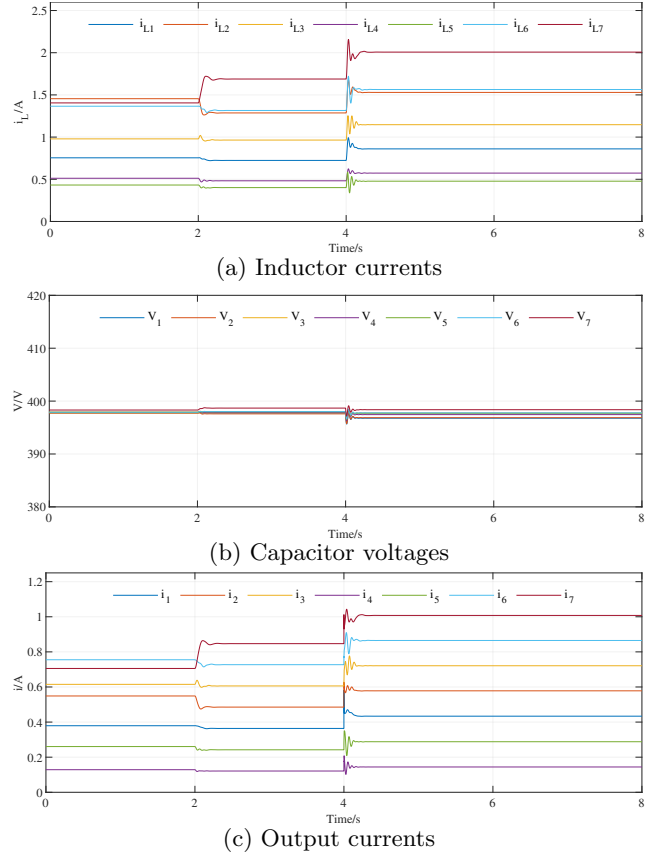


Fig. 4. Dynamic response of the meshed DC micro-grid system under primary and secondary controller

5.1.1 Secondary control enable, load increase and communication failure

The dynamic behaviour of the meshed micro-grid system when enabling the secondary controller, increasing the loads power demand, and experiencing a communication failure is shown in Fig. 4. During the first 2 s , the converters under primary control only are feeding the local CPLs, with the requested local power given by the power vector $P = [100\ 300\ 200\ 50\ 300\ 250\ 150]\text{ W}$. The output voltages remain closely regulated to $V^* = 400\text{ V}$ (Fig. 4b), with the input currents below their imposed limits (Fig. 4a), while in Fig. 4c the power injected in the network clearly does not satisfy the distribution agreement chosen to be $7 : 6 : 5 : 4 : 3 : 2 : 1$.

To address the latter issue, at $t = 2\text{ s}$ the secondary controller is enabled. Instantly, the distribution of the injected power by each converter is improved, as one can observe in Fig. 4c, having the output current vector $i = [0.12\ 0.24\ 0.36\ 0.49\ 0.61\ 0.72\ 0.85]\text{ A}$. This also improves the output voltages, becoming slightly closer to the rated $V^* = 400$ value, as shown in Fig. 4b.

The requested power in the network increases at $t = 4\text{ s}$, with the local load power vector becoming $P = [200\ 330\ 200\ 75\ 300\ 275\ 225]\text{ W}$. The input currents increase to satisfy the new load power demand, but

remain below their imposed limits (Fig. 4a). In Fig. 4b, the output voltages decrease, with the lowest being $V_1 = 397V$; that is, a voltage drop of below 1%. The injected power keeps the accurate distribution among converters with the output current vector being $i = [0.145 \ 0.29 \ 0.43 \ 0.58 \ 0.72 \ 0.865 \ 1] A$ as seen in Fig. 4c.

A communication failure occurs at $t = 6s$. The communication link between converters 2 and 3 is disconnected. However, this fault does not affect the system performance as one can notice in Fig. 4, the system retaining the same dynamic behaviour as prior to the communication failure occurring.

5.1.2 Voltage fluctuations and converter loss

Renewable energy sources are well-known to exhibit unpredictable behaviour due to the variation of their availability. That is why, the controller performance is tested when unpredictable phenomena occurs (Fig. 5), such as input voltage fluctuations, or complete unit disconnection.

At time interval $0s - 2s$, the system is running under both primary and secondary control. The power injected into the network is accurately distributed by each converter (Fig. 5c), the output voltages are closely regulated to the rated value (Fig. 5b), while the input currents are kept within their limits as seen in Fig. 5a.

Over the following $4s$, converter 1 experiences a sudden input voltage drop of 10%, followed by quick voltage recovery. Hence, at time $t = 2s$, the input voltage of converter 1 drops by 10%. The input current i_{L1} increases to keep satisfying the accurate power distribution, given the value is still below its maximum limit $i_{L1} < i_{L1}^{max} = 5A$ (Fig. 5a). In Fig. 5b, the output voltage V_1 remains closely regulated to the rated value, seemingly unaffected by the input variation. Moreover, the power distribution of the all seven converters is kept accurate as shown in Fig. 5c, having the output current vector $i = [0.12 \ 0.24 \ 0.36 \ 0.48 \ 0.6 \ 0.72 \ 0.84] A$. The input voltage recovers to its nominal value at time $t = 4s$, and the system comes back to its initial running state.

Converter 7 is disconnected at $t = 6s$, and, following short transients in the input current that decreases and output voltage that increases to the rated $V^* = 400V$, converter 7 starts feeding its own load only. The output voltages of the remaining six converters in the network drop slightly (Fig. 5b), but the power distribution is kept accurate between them, having the output current vector $i = [0.145 \ 0.29 \ 0.43 \ 0.57 \ 0.72 \ 0.86] A$, as presented in Fig. 5c. This concludes the simulation part when having meshed network configuration.

5.2 Parallel micro-grid topology case

For the converters feeding a common load, the same ratio is kept for the output power among the sources, that is $7 : 6 : 5 : 4 : 3 : 2 : 1$. According to Fig. 3b, only converters 1 and 5 participate in the load voltage recovery, that is, the pinning control gains are set as $g_1 = g_5 = 1$ and $g_2 = g_3 = g_4 = g_6 = g_7 = 0$.

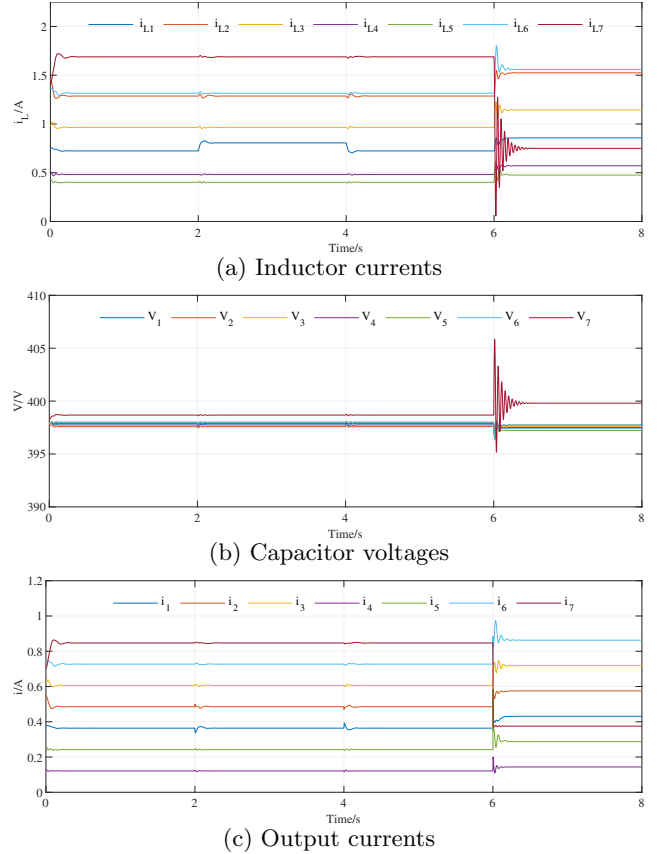


Fig. 5. Dynamic response of the meshed DC micro-grid system under voltage fluctuations and converter loss

5.2.1 Secondary control enable, load increase, current limitation and communication failure

The dynamic response of the parallel DC micro-grid system when enabling the secondary controller, increasing the load power demand, limiting the current and experiencing communication failure is presented in Fig. 6. During the first $2s$, the load power demand is $P = 4.2 kW$ and the system is controlled by the primary controller only. The load voltage is kept below the reference V^* , having $V_o \approx 392V$ as depicted in Fig. 6b.

Table 1
System and control parameters for simulation testing

Parameters	Values
$U [V]$	[200 150 250 100 240 220 200]
$C [\mu F]$	[700 400 500 100 150 450 490]
$R [\Omega]$	[0.5 1.5 1 0.7 1.2 0.8 0.65]
$L [mH]$	[2.3 2.2 2 2 2.5 2.1 2]
k	[1.8 2 2.5 1 1.9 1.8 1.5]
$m \times 10^{-2}$	[1.4 1.05 0.84 4.2 2.1 0.7 0.6]
E_{max}	[25 35 32 18 24 30 36]
r_v	[5 5 4 3 2 3 3]
α, β	100, 10

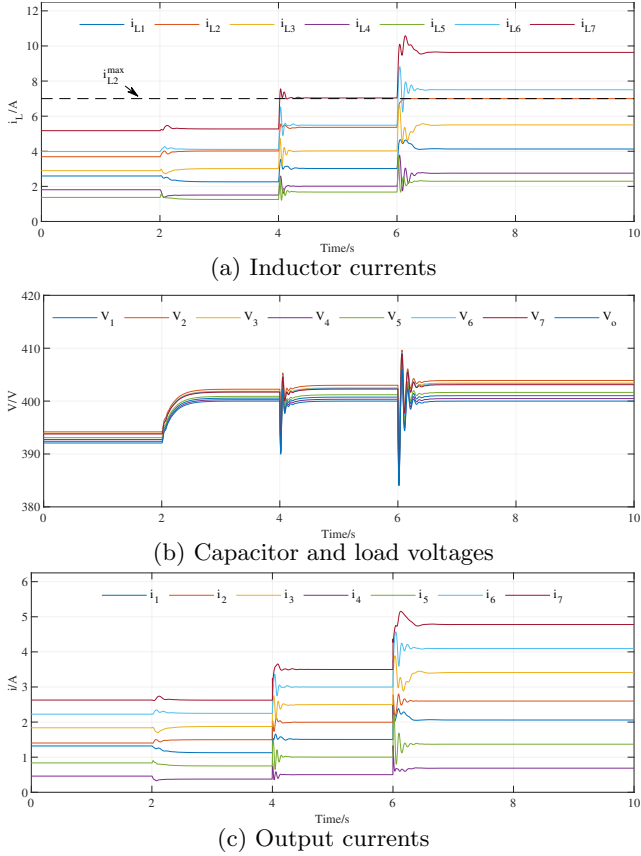


Fig. 6. Dynamic response of the parallel DC micro-grid system under primary and secondary controller

Also, it is clear from Fig. 6c, that the power sharing is not accurate, since the output currents are not proportional, i.e. $i \approx [2.63 \ 2.23 \ 1.84 \ 1.4 \ 1.32 \ 0.84 \ 0.46] \text{ A}$.

At $t = 2 \text{ s}$, the secondary controller is enabled, enhancing the performance of the system with the load voltage tightly regulated to the reference, $V_o = V^* = 400 \text{ V}$ (Fig. 6b), and the power sharing becoming very accurate with proportional output currents being $i \approx [2.62 \ 2.25 \ 1.87 \ 1.5 \ 1.13 \ 0.75 \ 0.376] \text{ A}$ as one can notice in Fig. 6c, given the inductor currents being below their maximum technical limit as depicted in Fig. 6a.

The load power demand increases to $P = 5.6 \text{ kW}$, at $t = 4 \text{ s}$. In Fig. 6b, one can see that the load voltage remains at the desired 400 V value, while the output currents are still accurately shared, in Fig. 6c, having proportional values $i \approx [3.5 \ 3 \ 2.5 \ 2 \ 1.5 \ 1 \ 0.5] \text{ A}$.

In order to test the overcurrent protection, the system is required, at $t = 6 \text{ s}$, to feed an increased load of 7.6 kW . The load voltage stays fixed at 400 V (Fig. 6b). But, the inductor current of the second converter, i_{L2} , reaches its $i_{L2}^{max} = 7 \text{ A}$ limit (Fig. 6a), and as a consequence, the converter loses its power sharing. However, the power sharing is kept between the other six converters in a $7 : 6 : 5 : 3 : 2 : 1$ ratio (Fig. 6c), having $i \approx [4.78 \ 4.09 \ 3.41 \ 2.06 \ 1.37 \ 0.69] \text{ A}$.

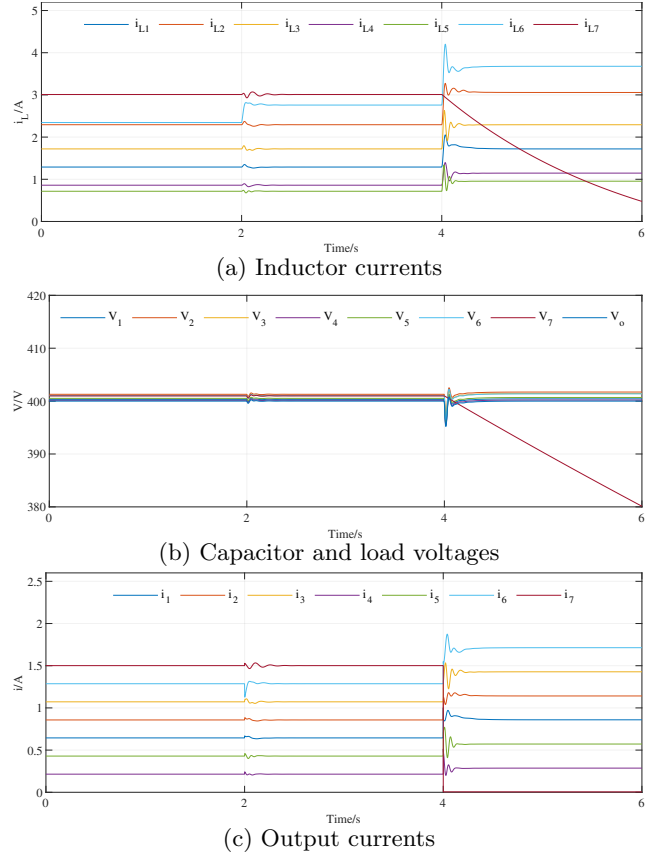


Fig. 7. Dynamic response of the parallel DC micro-grid system under voltage fluctuations and converter loss

So as to investigate the influence of the possible communication failures on the performances of the proposed method, at $t = 8 \text{ s}$, the communication network is subjected to three faults. The link that connects converter 1 to the common bus is disconnected ($g_1 = 0$), and also the connections between converters 5 to 6, and 6 to 7 are disrupted. In Figures 6b and 6c, one can observe that the voltage remains at the desired V^* value and the power sharing is unaffected by the communication failure.

5.2.2 Voltage fluctuations and converter loss

In this subsection, the effect of input voltage fluctuations is investigated under primary and secondary controller. Additionally, the event of a complete disconnection of a converter from the main bus is included, for the same case study.

Over the first 2 s , the converters operate under primary and secondary control feeding a 2.4 kW load. It can be observed in Fig. 7b that the voltage regulation is very accurate with $V_o = 400 \text{ V}$, while the output currents are accurately shared having $i \approx [0.21 \ 0.43 \ 0.64 \ 0.86 \ 1.07 \ 1.29 \ 1.50] \text{ A}$.

At $t = 2 \text{ s}$, converter 6 experiences a 15% input voltage drop. After a short transient, the voltage regulation and power sharing return back to their previous accurate

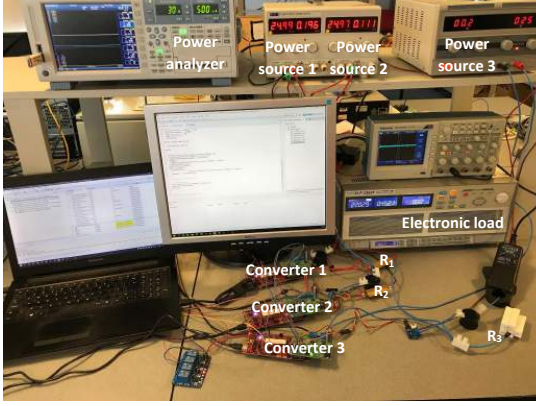


Fig. 8. Experimental testbed

Table 2
System and control parameters for experimental testing

Parameters	Values	Parameters	Values
U [V]	[24 24 24]	m	$[3\ 6\ 6] \times 10^{-3}$
C [μF]	[100 100 100]	E_{max}	[10 9 10]
R [Ω]	[1 1 2.3]	r_v	[5 6 5]
L [mH]	[2.2 2.2 2.2]	α	2
k	[5 5 10]	β	1

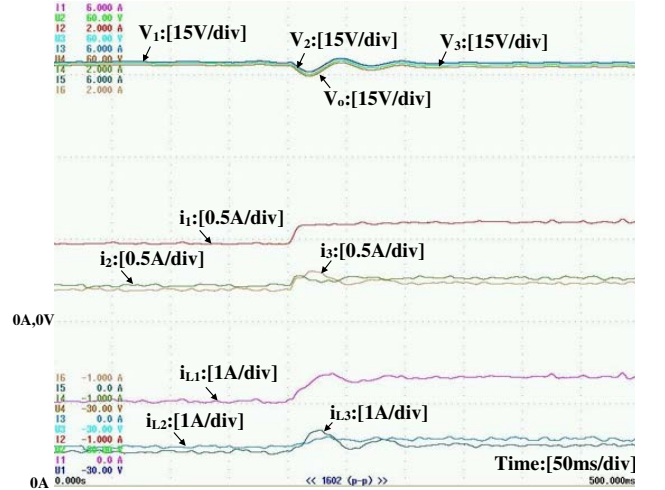
values since the load remained constant. However, one can notice, in Fig. 7a, that the input current of converter 6 increases to satisfy the amount of power required to keep the power sharing accurate.

Later on, at $t = 4$ s, converter 7 is disconnected from the network. The input current i_{L7} tends to zero (Fig 7a), and also the output voltage V_7 starts decreasing (Fig 7b), but the load voltage stays tightly regulated to 400 V. In Fig. 7c, it can be observed that the remaining currents stay accurate in a 6 : 5 : 4 : 3 : 2 : 1 ratio, with $i \approx [0.285\ 0.57\ 0.86\ 1.14\ 1.42\ 1.71]$ A.

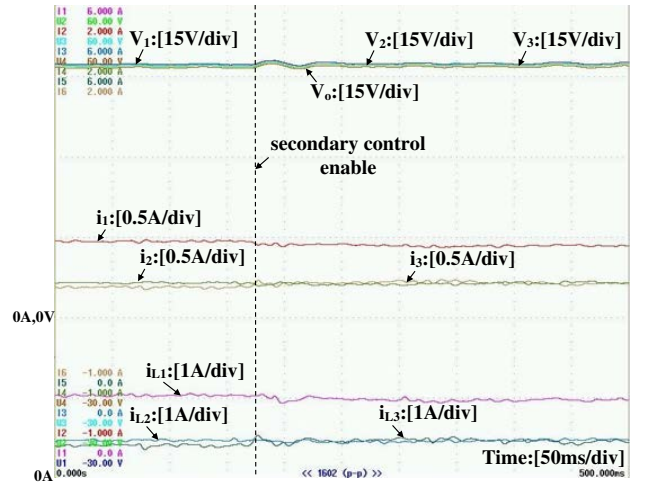
6 Experimental results

For experimental testing, the DC micro-grid displayed in Fig. 8 is considered, consisting of three Texas Instruments modules operated as DC/DC boost converters and feeding a common ETPS ELP-3362F electronic load acting as a CPL, with the parameters given in Table 2. The main tasks of the primary and secondary controllers are to regulate the output voltage to $V^* = 48$ V, while keeping a proportional 1 : 1 : 2 output load power sharing, provided none of the converters violate their maximum allowed input current, imposed by their technical requirements. The filtered dynamic response of the output voltages and input/output currents is captured in Fig. 9.

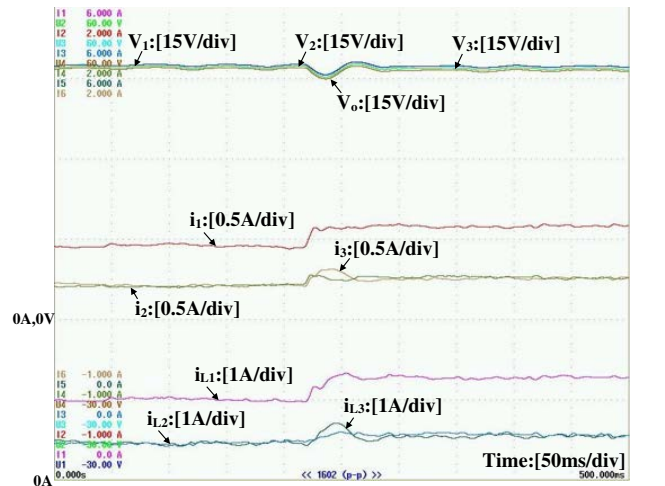
In Fig. 9a, under primary control only, the load power demand increases from 40 W to 50 W. One notices that the power sharing is not accurately kept in a 1 : 1 : 2 ratio, having $i \approx [0.18\ 0.21\ 0.47]$ A when the load is 40 W, and $i \approx [0.23\ 0.26\ 0.60]$ A when it increases to 50 W. Furthermore, the load voltage regulation decreases from $V_o \approx 46.6$ V, as it was initially,



(a) Load power demand increases from 40W to 50W under primary control



(b) Dynamic response when enabling the secondary control



(c) Load power demand increases from 40W to 50W under primary and secondary control

Fig. 9. Experimental results of the DC micro-grid system under primary and secondary controller

down to $V_o \approx 45.9V$ following the load change.

The dynamic response when enabling the secondary control is captured in Fig. 9b, while maintaining the load power demand constant at $40W$. It becomes clear that when the secondary controller is enabled, the accuracy of the power sharing is improved, reaching the desired proportional $1 : 1 : 2$ sharing, having $i \approx [0.22 \ 0.22 \ 0.44] A$. Moreover, the load voltage rises and becomes closer to the rated value V^* compared to the case where only the primary control is applied.

To highlight the superiority of the combined primary and secondary control under power demand variation, the same load power change is performed, from $40W$ to $50W$. The dynamic response is presented in Fig.9c. Unlike case (a), the voltage regulation is tighter, i.e. the output voltage V_o is closer to V^* , while the improved output currents maintain their $1 : 1 : 2$ desired sharing, with $i \approx [0.27 \ 0.27 \ 0.55] A$.

7 Conclusions

A novel decentralised primary and distributed secondary control was proposed to achieve accurate power sharing, voltage regulation, input current limitation and overcome the CPL instability problem. By employing singular perturbation theory and two time-scale analysis, the closed-loop system stability was analytically proven, taking into account both the physical system and the two-level control dynamics. Both simulation and experimental testings were carried out to validate the presented approach and analysis.

Future research will focus on the implementation of the proposed control scheme with different converter types, and on the effect of communication delays on the stability of the entire system. The scenario where the line inductance is considered that would pose the non-trivial challenge of computing the solutions of the load voltage is also an open problem for future investigation.

Acknowledgements

This work is supported by the Engineering and Physical Sciences Research Council (EPSRC) under Grant EP/S001107/1 and Grant EP/S031863/1, and under Grant 81359 from the Research Committee of the University of Patras via "C.CARATHEODORY" program.

APPENDIX

A Proof of Lemma 3

Matrix SD is similar to the symmetric matrix $D^{\frac{1}{2}}(SD)D^{-\frac{1}{2}} = D^{\frac{1}{2}}SD^{\frac{1}{2}}$, hence it is diagonalizable. This proves conclusion (a). By employing polar decomposition SD (or DS) can be written as $SD = UP$, where U is unitary and $P = \sqrt{(SD)^*SD}$ is an unique positive-semidefinite Hermitian matrix. Define Q to satisfy $Q^2 = U$ (see Garcia & Horn (2017, Ch.12)). Note that $M = Q^{-1}(SD)Q = QPQ$ is Hermitian, hence, by eigendecomposition $M = V\Lambda V^{-1}$, with V unitary and Λ diagonal with the eigenvalues of M (and

the same index of inertia as SD) as main diagonal entries. It can be concluded that $(QV)^{-1}SD(QV) = \Lambda$, with QV unitary according to Lemma 2.

As the similarity transformation $D^{\frac{1}{2}}(SD)D^{-\frac{1}{2}} = D^{\frac{1}{2}}SD^{\frac{1}{2}}$ is congruent to S ; then, according to Sylvester's law of inertia, SD has the same index of inertia as matrix S . The proof of conclusion (b) is shown in Meyer (2000, Ch.7). \square

B Proof of Lemma 4

Since \mathcal{G} is connected and there exists at least a single non-zero entry in y , then \mathcal{G}^\dagger is also connected. Thus, \mathcal{G}^\dagger has at least one spanning tree, and by Kirchhoff's Theorem, any minor of \mathcal{L}^\dagger is positive. That is, $|\mathcal{L} + \Delta| > 0$ and since both \mathcal{L} and Δ are positive semi-definite, which excludes the possibility of pair-wise negative eigenvalues, then $\mathcal{L} + \Delta$ is positive-definite.¹ \square

C Proof of Corollary 1

As the Laplacian \mathcal{L}_{cyb} is balanced and symmetric, $\ker(\mathcal{L}_{cyb}) = \text{span}(\mathbf{1}_n)$. That is $\mathbf{1}_n^T \mathcal{L}_{cyb} = \mathbf{0}_n^T$. Hence, by left multiplication with $\mathbf{1}_n^T$, equation (21) becomes

$$\alpha \mathbf{1}_n^T g(V^* - V_o) - \beta \mathbf{1}_n^T \mathcal{L}_{cyb} m P_{inj} = \mathbf{0}_n. \quad (\text{C.1})$$

As the right term in (C.1) is $\mathbf{0}_n$, equality (23) holds if $\sum_{i=1}^n g_i \neq 0$, or equivalently $\sum_{i=1}^n g_i > 0$, given that $g_i \geq 0, \forall i \in \mathcal{I}$. By substituting (23) into (21), it yields

$$\beta \mathcal{L}_{cyb} m P_{inj} = \mathbf{0}_n.$$

One can easily see that $m P_{inj} \in \text{span}(\mathbf{1}_n)$, since it is equivalent to (22). This completes the proof. \square

D Proof of Lemma 5

By employing the QEP theory for the symmetric matrix $-X_2$, one obtains

$$|\lambda I_{2n} + X_2| = |\lambda^2 \mathbb{T} + \lambda \mathbb{F} + \mathbb{S}| = 0 \quad (\text{D.1})$$

By left multiplying (D.1) with $m^{-1} [V_e]^{-1} \succ 0$, one gets

$$|\lambda^2 \bar{\mathbb{T}} + \lambda \bar{\mathbb{F}} + \bar{\mathbb{S}}| = 0 \quad (\text{D.2})$$

where $\bar{\mathbb{T}} = m^{-1} [V_e]^{-1} \succ 0$ and

$$\bar{\mathbb{F}} = m^{-1} [V_e]^{-2} (V^* I_n + [e]) + \mathcal{L} + m^{-1} [V_e]^{-1} \quad (\text{D.3})$$

$$\bar{\mathbb{S}} = m^{-1} [V_e]^{-2} (V^* I_n + [e]) + \mathcal{L} - m^{-1} [V_e]^{-1} \quad (\text{D.4})$$

Since matrix $\bar{\mathbb{T}}$ is already positive-definite, if the remaining matrices $\bar{\mathbb{F}}$ and $\bar{\mathbb{S}}$ are positive-definite, then $-X_2$ is negative-definite, hence X_2 is positive-definite. Condition $\bar{\mathbb{F}} \succ 0$ is satisfied since it is represented by a sum of two positive-definite matrices and the positive

¹ To prove that $\mathcal{L} + \Delta \succ 0$, one can equivalently show that the null-spaces of \mathcal{L} and Δ exclude any non-zero vector at their intersection.

semi-definite matrix \mathcal{L} . By virtue of Lemma 1, $\bar{\mathbb{S}} \succ 0$ holds if the following condition in scalar form

$$\frac{V^* + e_{ie}}{m_i V_{ie}^2} + \lambda_{\mathcal{L}i} - \frac{1}{m_i V_{ie}} > 0 \quad (\text{D.5})$$

is satisfied. By factorising, it yields

$$\frac{1}{m_i V_{ie}} \left(\frac{V^* + e_{ie}}{V_{ie}} - 1 \right) + \lambda_{\mathcal{L}i} > 0 \quad (\text{D.6})$$

where $\lambda_{\mathcal{L}i} \geq 0$ represents the eigenvalues of the Laplacian matrix \mathcal{L} . Considering a worst-case scenario, where $\lambda_{\mathcal{L}i} = 0$, the inequality in (D.6) will always hold since $\frac{V^* + e_{ie}}{V_{ie}} > 1$ is guaranteed by the droop equation (11) at steady state. Thus $X_2 \succ 0$, and since $X_1 \succeq 0$, by virtue of Lemma 3, $X_1 X_2$ (or $X_2 X_1$) is diagonalizable i.e. $P_1^{-1} J_3 P_1 = \Lambda_1$, with P_1 unitary and Λ_1 diagonal having real eigenvalues and same index of inertia as X_1 .

Hence, the proof of Lemma 5 is complete. \square

E Proof of Theorem 1

From the proof of Lemma 5, X_2 is positive-definite, with $\ker(X_2) = \mathbf{0}_{2n}$. Note that matrix X_1 is positive semi-definite, having $\ker(X_1) = \text{span}\left([\mathbf{0}_n^T \mathbf{1}_n^T]^T\right)$ corresponding to the global synchronization of the graph. Since $\text{Im}(\mathcal{L}_{cyb}) = \mathbf{1}_n^\perp$, $\text{Im}(X_2) \cap \ker(X_1) = \mathbf{0}_{2n}$, that is, $\text{Im}(X_2)$ excludes $\text{span}\left([\mathbf{0}_n^T \mathbf{1}_n^T]^T\right)$ or $X_1 \bar{v}$ is never in the kernel of X_2 . Thus one concludes that $\ker(\bar{J}_3) = \ker(X_1)$, which corresponds to global synchronization of the graph. By virtue of Simpson-Porco et al. (2013, Th.8), applying the Courant-Fischer Theorem to the eigenvalue problem (35), for global synchronization of the graph, all eigenvalues of \bar{J}_3 are real and negative.

The diagonal matrix Q_1 and its similar transformation \bar{Q}_1 are isospectral, having n null eigenvalues and n positive eigenvalues of the form $\lambda_{1\dots n}(\bar{Q}_1) = \frac{P_i}{C_i V_i^2}$. One can notice that multiplying \bar{Q}_1 by $\bar{v} = [\mathbf{0}_n^T \mathbf{1}_n^T]^T$ would yield eigenvalues outside of the matrix spectrum. Thus, $\bar{v} = [\mathbf{0}_n^T \mathbf{1}_n^T]^T$ is not an eigenvector of \bar{Q}_1 , and, hence, not an eigenvector of $\bar{J}_{2,\alpha=0}$. That is, it does not belong in the eigenspace of the Jacobian matrix $\bar{J}_{2,\alpha=0}$, i.e. $\bar{v} \notin N(\bar{J}_{2,\alpha=0} - \lambda I_{2n})$.

One can express $\tilde{J}_{2,\alpha=0} = (P_1^{-1} X_2^{-1}) \bar{J}_{2,\alpha=0} (X_2 P_1)$, thus the SEP becomes as follows

$$(-\beta \Lambda_1 + P_1^{-1} Q_1 P_1) \bar{z} = \lambda \bar{z} \quad (\text{E.1})$$

having matrix Λ_1 diagonal, unitarily similar to $X_2 X_1$ as shown in Lemma 4, and $P_1^{-1} Q_1 P_1$ symmetrical, isospectral with matrix Q_1 . Lemma 1 can be applied for the above SEP, yielding

$$-\beta \min_{\bar{z}^T \bar{z} \neq 0} \frac{\bar{z}^T \Lambda_1 \bar{z}}{\bar{z}^T \bar{z}} + \frac{P_i}{C_i V_i^2} < 0. \quad (\text{E.2})$$

This condition is always satisfied with an appropriate choice of the gain β , given to satisfy (36), in which case matrix $\tilde{J}_{2,\alpha=0}$ is Hurwitz, and by similarity also $\bar{J}_{2,\alpha=0}$ and $J_{2,\alpha=0}$. Then there exist $\rho_2 > 0$ and a domain $\tilde{D}_x = \{x \in R^{2n}, \|x\|_2 < \rho_2\}$ where $\tilde{D}_x \subseteq D_x$ such that the reduced model is exponentially stable at the origin.

This concludes the proof of Theorem 1. \square

F Proof of Lemma 6

Matrix X_4 is symmetric and singular, having $2n-1$ null eigenvalues, i.e. $\lambda_{1\dots 2n-1}(X_4) = 0$, and one positive eigenvalue equal to its trace, i.e. $\lambda_{2n}(X_4) = \text{Tr}(X_4) = n$. Hence X_4 is positive semi-definite.

To prove that the symmetric matrix X_3 is positive-definite, one uses again the quadratic eigenvalue problem (QEP) theory for matrix $-X_3$. This yields

$$|\lambda I_{2n} + X_3| = |\lambda^2 \mathbb{M} + \lambda \mathbb{C} + \mathbb{K}| = 0 \quad (\text{F.1})$$

where $\mathbb{M} = I_n \succ 0$ and

$$\mathbb{C} = \frac{1}{\alpha} (C^{-1} R^{-1} + I_n) \quad (\text{F.2})$$

$$\mathbb{K} = \frac{1}{\alpha^2} C^{-1} R^{-1} - \alpha^2 g^2 \quad (\text{F.3})$$

If \mathbb{M} , \mathbb{C} and \mathbb{K} are positive-definite, then $\text{Re}(\lambda) < 0$, and $-X_3$ is negative-definite, thus X_3 is positive-definite. The first condition $\mathbb{C} \succ 0$ is easily satisfied, given that $\alpha > 0$. Regarding the second condition $\mathbb{K} \succ 0$, since it consists of a sum of two diagonal matrices, using Lemma 1 in Su et al. (2018), the condition, in scalar form, becomes

$$\frac{1}{\alpha^2 C_i R_i} - \alpha^2 g_i^2 > 0, \forall i \in \mathcal{I} \quad (\text{F.4})$$

with the pinning control gain g_i either 0 or 1. Assuming a worst case scenario, $g_i = 1$, the above inequality holds given an appropriate selection for α as specified in (39).

As X_3 is a positive definite symmetric matrix, and X_4 is a positive semi-definite symmetric matrix, then according to Lemma 3,

1) $X_3 X_4$ (or $X_4 X_3$) is diagonalizable, i.e. $P_2^{-1} \bar{J}_4 P_2 = \Lambda_2$, with P_2 unitary and Λ_2 diagonal having the same index of inertia as matrix \bar{J}_4 , and

2) the eigenvalues of $X_3 X_4$ are real, and $X_3 X_4$ has the same number of positive (zero, or negative) eigenvalues with matrix X_4 .

Hence, the proof of Lemma 6 is complete. \square

G Proof of Lemma 7

Matrix \bar{J}_5 can be split into a product of two symmetric matrices, X_1 and $X_5 Q_2^{-1}$. The latter symmetric matrix, $X_5 Q_2^{-1}$, has the following shape

$$X_5 Q_2^{-1} = \begin{bmatrix} [V_e]^{-1} (V^* I_n + [e]) D^{-1} + [V_e] m R^{-1} D^{-1} & -D^{-1} \\ -D^{-1} & D^{-1} \end{bmatrix}$$

By applying the QEP theory again for the matrix $-X_5Q_2^{-1}$, we get

$$|\lambda I_n + X_5Q_2^{-1}| = |\lambda^2 \mathbb{N} + \lambda \mathbb{E} + \mathbb{L}| = 0 \quad (\text{G.1})$$

where $\mathbb{N} = I_n \succ 0$ and

$$\mathbb{E} = [V_e]^{-1}(V^*I_n + [e])D^{-1} + [V_e]mR^{-1}D^{-1} + D^{-1} \quad (\text{G.2})$$

$$\mathbb{L} = [V_e]^{-1}(V^*I_n + [e])D^{-2} + [V_e]mR^{-1}D^{-2} - D^{-2} \quad (\text{G.3})$$

If the conditions $\mathbb{N} \succ 0$, $\mathbb{E} \succ 0$ and $\mathbb{L} \succ 0$ hold, then $\text{Re}(\lambda) < 0$, and $-X_5Q_2^{-1}$ is negative-definite, thus $X_5Q_2^{-1}$ is positive-definite. Condition $\mathbb{E} \succ 0$ is satisfied as it represents a positive-definite diagonal matrix. Condition $\mathbb{L} \succ 0$ will hold, according to Lemma 1, if the following condition in scalar form is guaranteed

$$\left(\frac{1}{V_{ie}} (V^* + e_{ie}) + \frac{V_{ie}m_i}{R_i} - 1 \right) \frac{1}{\lambda_{Di}^2} > 0, \forall i \in \mathcal{I} \quad (\text{G.4})$$

which is easily satisfied since $\frac{V^* + e_{ie}}{V_{ie}} > 1$ from the droop equation (11) at the steady state. Thus, $X_5Q_2^{-1} \succ 0$, and since $X_1 \succeq 0$, then \tilde{J}_5 is diagonalizable, according to Lemma 3, i.e. $P_3^{-1}\tilde{J}_5P_3 = \Lambda_3$, with P_3 unitary and Λ_3 diagonal having the same index of inertia as matrix \tilde{J}_5 .

This completes the proof of Lemma 7. \square

H Proof of Theorem 2

As already mentioned, matrix X_1 is semi-positive definite with kernel spanned by $[\mathbf{0}_n^T \mathbf{1}_n^T]^T$ corresponding to the global synchronization of the graph, while matrix $X_5Q_2^{-1}$ is positive definite with kernel spanned by $\mathbf{0}_{2n}$. Following the proof in Simpson-Porco et al. (2013, Th.8), by applying the Courant-Fischer Theorem to the eigenvalue problem, for global synchronization of the graph, all eigenvalues of \tilde{J}_5 are real and negative since $\text{Im}(\mathcal{L}) = \mathbf{1}_n^\perp$, and $\text{Im}(X_5Q_2^{-1}) \cap \ker(X_1) = \mathbf{0}_{2n}$, which means that $X_1\bar{u}$ is never in the kernel of $X_5Q_2^{-1}$. Hence, one can see that $\ker(\tilde{J}_5) = \ker(X_1)$. As the image of the matrix $X_5Q_2^{-1}$ excludes $\text{span}\left([\mathbf{0}_n^T \mathbf{1}_n^T]^T\right)$, it follows that $\tilde{J}_5\bar{u}$ is the zero vector if and only if $\bar{u} \in \text{span}\left([\mathbf{0}_n^T \mathbf{1}_n^T]^T\right)$ that corresponds to the global synchronization of the graph.

Matrices \bar{J}_4 and \tilde{J}_4 have the same spectrum, that is, they have $2n - 1$ null eigenvalues and one positive eigenvalue. It is important to underline that multiplying \tilde{J}_4 with vector $\bar{u} = [\mathbf{0}_1 \mathbf{1}_n]$ would render a value outside of the matrix spectrum. Hence, one can conclude that $\bar{u} = [\mathbf{0}_n^T \mathbf{1}_n^T]^T$ is not an eigenvector of \tilde{J}_4 , and hence, not an eigenvector of $\tilde{J}_{2,\alpha \neq 0}$. That is, vector $\bar{u} = [\mathbf{0}_1 \mathbf{1}_n]$ does not belong in the eigenspace of the Jacobian matrix $\tilde{J}_{2,\alpha \neq 0}$, i.e. $\bar{u} \notin N\left(\tilde{J}_{2,\alpha \neq 0} - \lambda I_{2n}\right)$.

Consider matrix \bar{J}_4 for which there is

$$\bar{J}_4\bar{w} = \lambda\bar{w} \quad (\text{H.1})$$

with λ the eigenvalue of \bar{J}_4 , and \bar{w} the corresponding eigenvector. Following the similarity transformation in (40), there is $\tilde{J}_4\bar{u} = \lambda\bar{u}$, with \bar{u} given as

$$\bar{u} = (X_5Q_2^{-1})^{-1}\bar{w} \quad (\text{H.2})$$

Matrix $X_5Q_2^{-1}$ is given in Appendix G, while its inverse, $(X_5Q_2^{-1})^{-1}$, has the following expression

$$(X_5Q_2^{-1})^{-1} = \frac{1}{|\mathbb{L}|} \begin{bmatrix} D^{-1} & D^{-1} \\ D^{-1} [V_e]^{-1}(V^*I_n + [e]) & D^{-1} + [V_e]mR^{-1}D^{-1} \end{bmatrix} \quad (\text{H.3})$$

where \mathbb{L} is expressed in (G.3). Notice that (H.3) is also symmetric and positive-definite since $X_5Q_2^{-1} \succ 0$, according to Proposition 2. For \bar{u} given as $\bar{u} = [\mathbf{0}_n^T \mathbf{1}_n^T]^T$, then there is

$$(X_5Q_2^{-1})^{-1} \begin{bmatrix} \bar{w}_{n1} \\ \bar{w}_{n2} \end{bmatrix} = \begin{bmatrix} \mathbf{0}_n \\ \mathbf{1}_n \end{bmatrix} = \begin{bmatrix} \frac{1}{|\mathbb{L}|}(D^{-1})(\bar{w}_{n1} + \bar{w}_{n2}) \\ \frac{1}{|\mathbb{L}|}(D^{-1}\bar{w}_{n1} + [V_e]^{-1}(V^*I_n + [e])D^{-1} + [V_e]mR^{-1}D^{-1}\bar{w}_{n2}) \end{bmatrix}$$

which holds if $\bar{w}_{n1} = -\bar{w}_{n2}$. However, if $\bar{w} = [\bar{w}_{n1} \ -\bar{w}_{n1}]^T$, then from (H.1), eigenvector \bar{w} would yield a positive eigenvalue outside of the spectrum of matrix \bar{J}_4 . Thus, \bar{w} is not an eigenvector of \bar{J}_4 since the opposite implies that \bar{J}_4 has two non-zero eigenvalues, which would be in contradiction with the proof of Proposition 1. Therein, it is demonstrated that the index of inertia of \bar{J}_4 is $i(\bar{J}_4) = [1 \ 0 \ 2n - 1]$.

Therefore, it follows from Lemma 1, that if $\bar{u} = [\mathbf{0}_n^T \mathbf{1}_n^T]^T$ is not an eigenvector of matrix \tilde{J}_4 , then ultimately it is not an eigenvector of the Jacobian $\tilde{J}_{2,\alpha \neq 0}$.

Note that $J_6 = (P_2^{-1}Q_2X_5^{-1})\tilde{J}_{2,\alpha \neq 0}(X_5Q_2^{-1}P_2)$, isospectral with $\tilde{J}_{2,\alpha \neq 0}$, can be expressed as

$$J_6 = \alpha\Lambda_2 - \beta P_2^{-1}X_1X_5Q_2^{-1}P_2 \quad (\text{H.4})$$

Then, let the matrix $J_7 = P_4^{-1}J_6P_4$, isospectral with J_6 and $\tilde{J}_{2,\alpha \neq 0}$, with $P_4 = P_2^{-1}P_3$, unitary according to Lemma 2, such that the new SEP becomes

$$(\alpha P_4^{-1}\Lambda_2P_4 - \beta\Lambda_3)\bar{e} = \lambda\bar{e}. \quad (\text{H.5})$$

Thus, matrix $P_4^{-1}\Lambda_2P_4$ is symmetric, since P_4 is unitary, similar to Λ_2 , having the same index of inertia as X_3X_4 as shown in Lemma 6, and Λ_3 diagonal having the same index of inertia as $X_1X_5Q_2^{-1}$, as explained in Lemma 7. Lemma 1 can be applied for the eigenvalues problem as follows

$$\alpha \sum_{i=1}^n \frac{1}{\alpha C_i R_i} - \beta \min_{\bar{e}^T \bar{e} \neq 0} \frac{\bar{e}^T \Lambda_3 \bar{e}}{\bar{e}^T \bar{e}} < 0. \quad (\text{H.6})$$

or simply

$$\sum_{i=1}^n \frac{1}{C_i R_i} - \beta \min_{\bar{e}^T \bar{e} \neq 0} \frac{\bar{e}^T \Lambda_3 \bar{e}}{\bar{e}^T \bar{e}} < 0. \quad (\text{H.7})$$

The above condition is satisfied at all times, with a proper choice of the gain β , required to satisfy (42).

Hence, if condition (42) holds, matrix J_7 is Hurwitz, and by similarity both J_6 and $\tilde{J}_{2,\alpha \neq 0}$ are Hurwitz, the latter having the same index of inertia as $\bar{J}_{2,\alpha \neq 0}$ and $J_{2,\alpha \neq 0}$ (as mentioned in Remark 3). Then, there exist $\rho_3 > 0$ and a domain $\tilde{D}_x = \{x \in R^{2n}, \|x\|_2 < \rho_3\}$ where $\tilde{D}_x \subseteq D_x$ such that the reduced model is exponentially stable at the origin. This completes the proof. \square

References

- Anand, S. & Fernandes, B. G. (2013), ‘Reduced-order model and stability analysis of low-voltage DC microgrid’, *IEEE Transactions on Industrial Electronics* **60**(11), 5040–5049.
- Bidram, A., Davoudi, A., Lewis, F. L. & Qu, Z. (2013), ‘Secondary control of microgrids based on distributed cooperative control of multi-agent systems’, *IET Generation, Transmission Distribution* **7**(8), 822–831.
- Braitor, A. C., Konstantopoulos, G. C. & Kadiramanathan, V. (2020a), ‘Current-limiting droop control design and stability analysis for paralleled boost converters in DC microgrids’, *IEEE Transactions on Control Systems Technology* pp. 1–10.
- Braitor, A.-C., Konstantopoulos, G. & Kadiramanathan, V. (2020b), ‘Admittance matrix computation and stability analysis of droop controlled dc micro-grids with cpl’, *IFAC-PapersOnLine* **53**(2), 13525–13530. 21th IFAC World Congress.
- Braitor, A., Konstantopoulos, G. C. & Kadiramanathan, V. (2020c), ‘Stability analysis and nonlinear current-limiting control design for dc micro-grids with cpls’, *IET Smart Grid* **3**(3), 355–366.
- Buticchi, G., Costa, L. & Liserre, M. (2017), ‘Improving system efficiency for the more electric aircraft: A look at dcdc converters for the avionic onboard dc microgrid’, *IEEE Industrial Electronics Magazine* **11**(3), 26–36.
- Cairolì, P. & Dougal, R. A. (2013), ‘New horizons in DC shipboard power systems: New fault protection strategies are essential to the adoption of DC power systems.’, *IEEE Electrification Magazine* **1**(2), 38–45.
- Cingoz, F., Elrayyah, A. & Sozer, Y. (2017), ‘Plug-and-play nonlinear droop construction scheme to optimize islanded microgrid operations’, *IEEE Transactions on Power Electronics* **32**(4), 2743–2756.
- Coelho, E. A., Wu, D., Guerrero, J. M., Vasquez, J. C., Dragicevic, T., Stefanovic, C. & Popovski, P. (2016), ‘Small-signal analysis of the microgrid secondary control considering a communication time delay’, *IEEE Transactions on Industrial Electronics* **63**(10), 6257–6269.
- Gao, F., Kang, R., Cao, J. & Yang, T. (2019), ‘Primary and secondary control in dc microgrids: a review’, *Journal of Modern Power Systems and Clean Energy* **7**(2), 227–242.
- Garcia, S. R. & Horn, R. A. (2017), *A Second Course in Linear Algebra*, Cambridge Mathematical Textbooks, Cambridge University Press.
- Han, R., Tucci, M., Martinelli, A., Guerrero, J. M. & Ferrar-Trecate, G. (2019), ‘Stability analysis of primary plug-and-play and secondary leader-based controllers for dc microgrid clusters’, *IEEE Transactions on Power Systems* **34**(3), 1780–1800.
- H.K.Khalil (2014), *Nonlinear Systems*, third edn, Pearson.
- Huang, P. H., Liu, P. C., Xiao, W. & Moursi, M. S. E. (2015), ‘A novel droop-based average voltage sharing control strategy for DC microgrids’, *IEEE Transactions on Smart Grid* **6**(3), 1096–1106.
- Jia, H., Cao, X., Yu, X. & Zhang, P. (2007), A simple approach to determine power system delay margin, in ‘2007 IEEE Power Engineering Society General Meeting’, pp. 1–7.
- Jin, C., Wang, P., Xiao, J., Tang, Y. & Choo, F. H. (2014), ‘Implementation of hierarchical control in dc microgrids’, *IEEE Transactions on Industrial Electronics* **61**(8), 4032–4042.
- Jr., G. A. B. & Graves-Morris, P. (1996), *Pade approximants*, New York, NY, USA: Cambridge Univ. Press.
- Jung-Won Kim, Hang-Seok Choi & Bo Hyung Cho (2002), ‘A novel droop method for converter parallel operation’, *IEEE Transactions on Power Electronics* **17**(1), 25–32.
- Konstantopoulos, G. C. & Baldvisio-Monasterios, P. R. (2019), ‘State-limiting PID controller for a class of nonlinear systems with constant uncertainties’, *International Journal of Robust and Nonlinear Control* **n/a**(n/a).
- Liu, X., Zhou, Y., Zhang, W. & Ma, S. (2011), ‘Stability criteria for constant power loads with multistage lc filters’, *IEEE Transactions on Vehicular Technology* **60**(5), 2042–2049.
- Liu, Z., Su, M., Sun, Y., Han, H., Hou, X. & Guerrero, J. M. (2018), ‘Stability analysis of dc microgrids with constant power load under distributed control methods’, *Automatica* **90**, 62 – 72.
- Loh, P. C., Blaabjerg, F., Peyghami-Akhuleh, S. & Mokhtari, H. (2016), Distributed secondary control in dc microgrids with low-bandwidth communication link, in ‘2016 7th Power Electronics and Drive Systems Technologies Conference (PEDSTC)’, pp. 641–645.
- Lu, X., Guerrero, J. M., Sun, K. & Vasquez, J. C. (2014), ‘An improved droop control method for dc microgrids based on low bandwidth communication with dc bus voltage restoration and enhanced current sharing accuracy’, *IEEE Transactions on Power Electronics* **29**(4), 1800–1812.
- Meyer, C. D. (2000), *Matrix Analysis and Applied Linear Algebra*, Society for Industrial and Applied Mathematics, Philadelphia.
- Milano, F. & Anghel, M. (2012), ‘Impact of time delays on power system stability’, *IEEE Transactions on Circuits and Systems I: Regular Papers* **59**(4), 889–900.
- Mohamed, Y. A. I. & El-Saadany, E. F. (2008), ‘Adaptive decentralized droop controller to preserve power sharing stability of paralleled inverters in distributed generation microgrids’, *IEEE Transactions on Power Electronics* **23**(6), 2806–2816.
- Nahata, P., Soloperto, R., Tucci, M., Martinelli, A. & Ferrar-Trecate, G. (2020), ‘A passivity-based approach to voltage stabilization in dc microgrids with zip loads’, *Automatica* **113**, 108770.
- Ortega, R., Loria, A., Nicklasson, P. J. & Sira-Ramirez, H. (1998), *Passivity-based Control of Euler-Lagrange Systems, Mechanical, Electrical and Electromechanical*

Applications, Springer-Verlag, Great Britain.

- Polyakov, A., Efimov, D., Perruquetti, W. & Richard, J. (2015), 'Implicit lyapunov-krasovski functionals for stability analysis and control design of time-delay systems', *IEEE Transactions on Automatic Control* **60**(12), 3344–3349.
- Salomonsson, D., Soder, L. & Sannino, A. (2008), 'An adaptive control system for a dc microgrid for data centers', *IEEE Transactions on Industry Applications* **44**(6), 1910–1917.
- Setthapun, W., Srikaew, S., Rakwichian, J., Tantranont, N., Rakwichian, W. & Singh, R. (2015), The integration and transition to a dc based community: A case study of the smart community in chiang mai world green city, in '2015 IEEE First International Conference on DC Microgrids (ICDCM)', pp. 205–209.
- Shafee, Q., Guerrero, J. M. & Vasquez, J. C. (2014), 'Distributed secondary control for islanded microgrids—a novel approach', *IEEE Transactions on Power Electronics* **29**(2), 1018–1031.
- Shuai, Z., He, D., Fang, J., Shen, Z. J., Tu, C. & Wang, J. (2016), 'Robust droop control of DC distribution networks', *IET Renewable Power Generation* **10**(6), 807–814.
- Simpson-Porco, J. W., Dörfler, F. & Bullo, F. (2013), 'Synchronization and power sharing for droop-controlled inverters in islanded microgrids', *Automatica* **49**(9), 2603 – 2611.
- Simpson-Porco, J. W., Dörfler, F. & Bullo, F. (2017), 'Voltage stabilization in microgrids via quadratic droop control', *IEEE Transactions on Automatic Control* **62**(3), 1239–1253.
- Su, M., Liu, Z., Sun, Y., Han, H. & Hou, X. (2018), 'Stability analysis and stabilization methods of DC microgrid with multiple parallel-connected DC-DC converters loaded by CPLs', *IEEE Transactions on Smart Grid* **9**(1), 132–142.
- Tahim, A. P. N., Pagano, D. J., Lenz, E. & Stramosk, V. (2015), 'Modeling and stability analysis of islanded DC microgrids under droop control', *IEEE Transactions on Power Electronics* **30**(8), 4597–4607.
- Xia, M., Antsaklis, P. J., Gupta, V. & McCourt, M. J. (2015), 'Determining passivity using linearization for systems with feedthrough terms', *IEEE Transactions on Automatic Control* **60**(9), 2536–2541.
- Xu, G., Sha, D. & Liao, X. (2015), 'Decentralized inverse-droop control for input-series-output-parallel DC-DC converters', *IEEE Transactions on Power Electronics* **30**(9), 4621–4625.
- Zhao, J. & Dörfler, F. (2015), 'Distributed control and optimization in dc microgrids', *Automatica* **61**, 18 – 26.

Andrei-Constantin Braitor

received the B.Eng. degree in power systems engineering from Politehnica University of Timisoara, Romania, the M.Sc. degree in energy and power systems from University of Liverpool, U.K., and the Ph.D. degree in control and power systems from University of Sheffield, U.K., in 2015, 2016 and 2021, respectively.



Currently, he is a Research Associate with the Department of Automatic Control and Systems Engineering, The University of Sheffield, U.K.. His primary research interests are centred around nonlinear and networked systems, nonlinear control design and stability analysis, distributed and optimal control with applications in micro-grids and energy systems.

George C. Konstantopoulos

received his Dipl.Eng. and Ph.D. degrees in electrical and computer engineering from the Department of Electrical and Computer Engineering, University of Patras, Rion, Greece, in 2008 and 2012, respectively. From 2011 to 2012, he was an Electrical Engineer with the Public Power Corporation of Greece. Since 2013, he has been with the Department of Automatic Control and Systems Engineering, The University of Sheffield, U.K., holding the positions of Research Associate, Research Fellow, Lecturer and Senior Lecturer. Since 2019, he has been with the Department of Electrical and Computer Engineering, University of Patras, Greece, as an Associate Professor. He is an EPSRC UKRI Innovation Fellow in the priority area of cheap and clean energy technologies and he currently serves as an Associate Editor of the IET Smart Grid Journal and the International Journal of Systems Science. His research interests include nonlinear modeling, control and stability analysis of power converters in microgrid and smart grid applications, renewable energy systems and electrical drives. Dr. Konstantopoulos is a Member of the National Technical Chamber of Greece.



Visakan Kadiramanathan

received the B.A. degree in electrical and information sciences and the Ph.D. degree in information engineering from the Department of Engineering, University of Cambridge, U.K., in 1987 and 1992, respectively. Following brief postdoctoral research positions at the Universities of Surrey and Cambridge, he was appointed Lecturer at the Department of Automatic Control and Systems Engineering, University of Sheffield, Sheffield, U.K. He is currently a Professor in Signal and Information Processing and is also the Director of the Rolls-Royce University Technology Centre in Control, Monitoring, and Systems Engineering, Sheffield, U.K. He has published more than 200 papers in peer-reviewed journals and conferences. His research interests are in the areas of data driven modeling, signal processing, and control with applications in aerospace, biomedical, and other dynamic systems. He was a recipient of the 2012 PNAS (Proceedings of the National Academy of Science, USA) Cozzarelli Prize. Dr. Kadiramanathan is a past Editor in Chief of the International Journal of Systems Science and is the current Chair of the United Kingdom Automatic Control Council.

